Table 1. Cytokine concentrations in conditioned medium of cultured human skin fibroblasts

	Control (H11)	Control (H34)	NPC1 (UCH)	NPC2 (81027)
IFN-β	ND	ND	83	63
IL-6	1.4	17	2860	2040
IL-8	ND	ND	1560	2320
IL-17	27	55	21	52
TNFα	0.49	0.49	0.59	0.66
TGFβ	ND	0.08	0.04	0.15
G-CSF	15	14	16	36
GM-CSF	2.8	ND	4.4	7.5
M-CSF	121	212	411	977

Medium was collected from cells cultured in serum-free DMEM for 24 h and filtered through 0.22 mm pore filters. Concentrations of each cytokine were determined by ELISA. Units are picograms/milliliter. Shown are the mean values obtained in a single determination performed in duplicate. Similar results were obtained in another independent experiment. The following cytokines were at undetectable levels in all of the four cell lines: IFN-α, IFN-γ, IL-1α, IL-1β, IL-2, IL-4, IL-5, IL-10, IL-11, IL-12, IL-13, IL-18, and leptin. Soluble IL-6 receptor was also undetectable. G-CSF, Granulocyte colony-stimulating factor; GM-CSF, granulocyte–macrophage colony-stimulating factor; M-CSF, macrophage colony-stimulating factor; ND, not detectable.

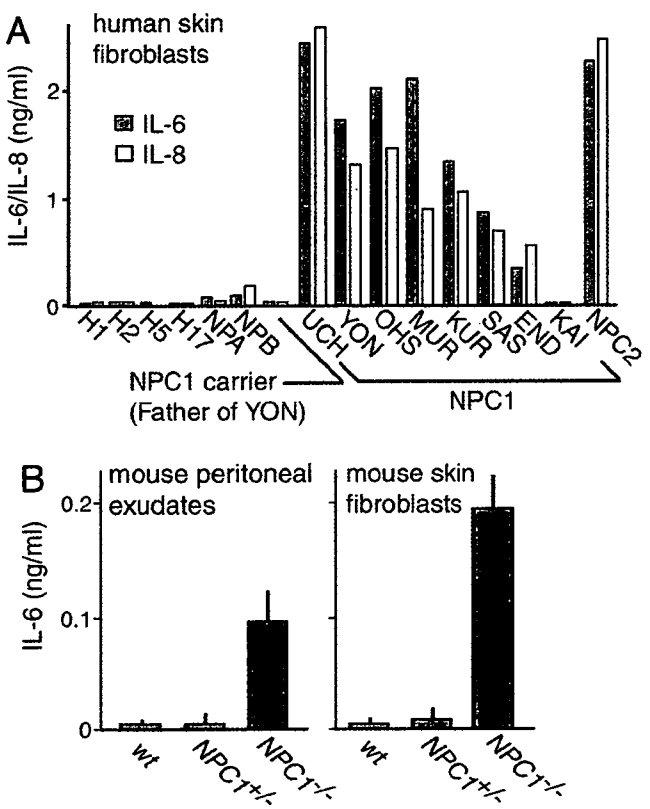

Figure 1. Secretion of IL-6 and IL-8 by NPC cells. ***A***, Secretion by human skin fibroblasts. Conditioned medium was prepared as described in Materials and Methods. Each bar represents the mean value of duplicates, obtained in a single experiment. Similar results were reproduced in another independent experiment. ***B***, Secretion by primary cultured mouse cells obtained from 6-week-old littermates. Peritoneal exudates were enriched for macrophages as described in Materials and Methods. Each bar represents the mean ± SEM of three determinations, each performed in duplicate.

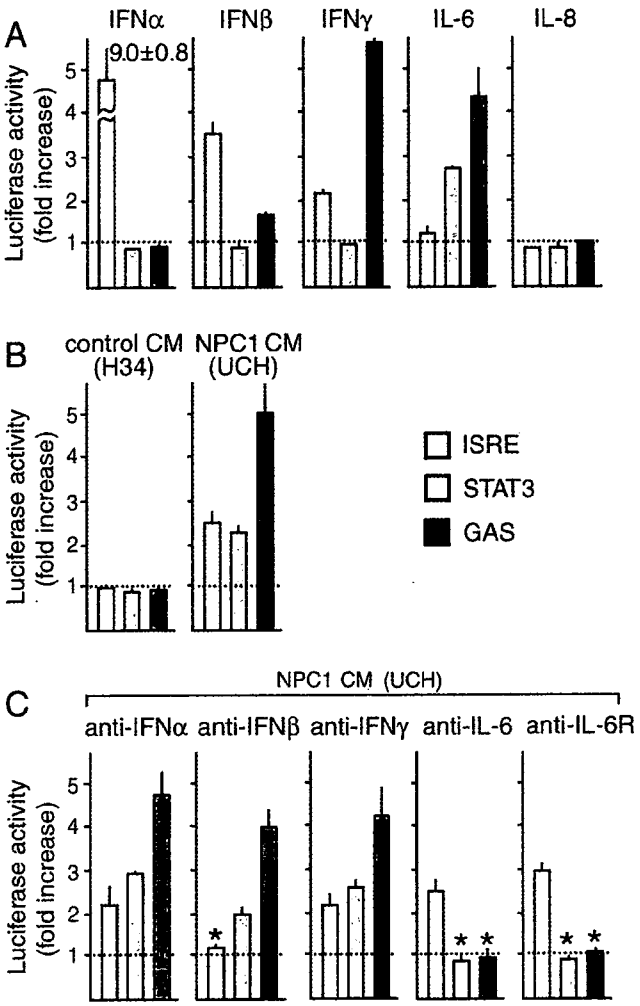

Figure 2. Activation of STATs by NPC cell CM assessed by reporter gene assays in HepG2 cells. Cells were transfected with a reporter construct containing each response element. ***A***, ***B***, At 24 h after transfection, they were stimulated for 6 h with recombinant cytokines (***A***) or CM of H34 or UCH cells (***B***). The concentration of each cytokine was 10 ng/ml. In ***C***, UCH CM was incubated with neutralizing antibodies at 37°C for 1 h before application. The concentration of each antibody was 2 μg/ml. Each bar represents the mean ± SEM of three determinations, each performed in triplicate. *$p < 0.01$, significantly different from the values without neutralization.

6 h in the same medium containing cytokines or conditioned medium. Luciferase activities in cell lysates were determined using Picagene kits (Toyo Ink, Tokyo, Japan), and GFP fluorescence was determined using a fluorophotometer (Perspective Biosystems, Framingham, MA). Human IFN-α and IFN-β were from PBL Biomedical Laboratories (Piscataway, NJ): IFN-γ, IL-6, and IL-8 were from Peprotech. Where indicated, conditioned medium was incubated at 37°C for 1 h with neutralizing antibodies against IFN-α, IFN-β, IFN-γ (PBL Biomedical Laboratories), IL-6, or IL-6 receptor (R&D Systems, Minneapolis, MN).

For NFκB reporter gene assays in HEK293 cells, cells were transfected with pNFκB-luc (Clontech) together with pEFBOS/TLR4 and/or MD-2. After incubation in DMEM/10% BCS for 24 h, cells were stimulated for 6 h with LPS or TNFα.

ELISA. Cytokines concentrations in conditioned media were determined by an ELISA assay (Biosource, Camarillo, CA) according to the manufacturer's instructions.

Generation of NPC mice that lack TLR4 or IL-6. BALB/c NPC mice and C57BL IL-6 knock-out mice were obtained from the The Jackson Laboratory (Bar Harbor, ME). C57BL TLR4 knock-out mice were a kind gift from Dr. S. Akira (Osaka University, Osaka, Japan). BALB/c NPC mice were backcrossed for four generations into the C57BL strain. Resultant $NPC1^{+/-}$ mice were crossed with $TLR4^{-/-}$ mice. Mice heterozygous for both *NPC1* and *TLR4* were intercrossed to generate $NPC1^{-/-}$ mice with TLR4 genotypes of *TLR4* +/+, +/−, and −/−. $NPC1^{-/-}$ mice with different IL-6 genotypes were generated in the same way. The genotype of each mouse was determined by genomic PCR. All experiments were performed according to Tottori University Animal Care and Use Committee guidelines.

Statistical analysis. Two-way ANOVA and Student's t test were used with $p < 0.05$ regarded as statistically significant.

Results

Increased secretion of IFN-β, IL-6, and IL-8 by NPC cells

Concentrations of 22 cytokines and soluble IL-6 receptor in serum-free conditioned medium (CM) were determined by ELISA using cells from two control subjects (H11 and H34), one patient (UCH) with NPC1 mutations, and another (81027) with NPC2 mutations (Table 1). Both UCH and 81027 had an infantile form of NPC (Yamamoto et al., 2000; Millat et al., 2001). The secreted cytokine profiles were remarkably similar between UCH and 81027 cells. Most significantly, secretion of IL-6 and IL-8 was markedly increased. Of the three IFNs, only IFN-β was detectable. Other detectable cytokines included IL-17, TNFα, transforming growth factor β (TGFβ), and three types of colony-stimulating factors (CSFs), whose concentrations were unaltered or marginally increased in NPC cells.

To confirm these results, we determined the concentrations of IL-6 and IL-8 in CM of cells from seven other patients with NPC1 mutations. Of these subjects, SAS and END had a juvenile form, KAI had an adult form, and all others had an infantile form (Yamamoto et al., 2000). IL-6/IL-8 levels were increased except for KAI (Fig. 1*A*). Their levels were marginally increased in cells from patients with NPA and NPB, but not in cells from four other control subjects, or from an NPC1 heterozygote. We also measured concentrations of IL-6 in CM of primary cultured peritoneal exudates enriched for macrophages and skin fibroblasts obtained from NPC mice. In both types of cell preparations, there was a clear increase in *NPC1*$^{-/-}$ cells compared with the levels in heterozygous and wild-type (*wt*) cells (Fig. 1*B*). Concentrations of IFN-β and IL-8 were not determined in the mouse samples because an ELISA was not available. Thus, the increased secretion of IL-6 appeared to be a common feature of NPC cells.

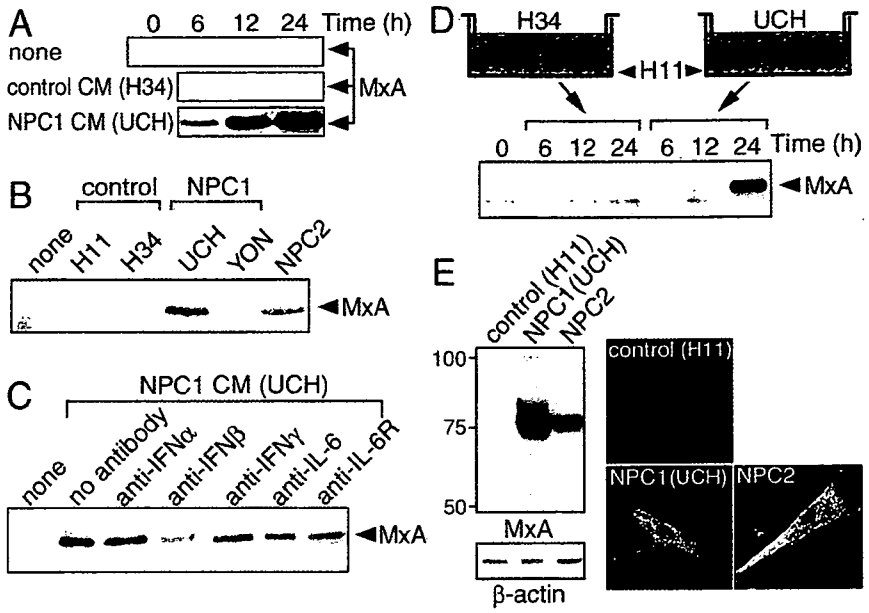

Figure 3. Activity of NPC cell CM to induce expression of MxA. In ***A–D***, MxA protein in H11 cells was detected by anti-MxA Western blotting. NPC cells were from patients with NPC1 mutations (UCH and YON) and NPC2 mutations (81027). ***A***, Time-dependent effects of UCH CM. H11 cells were incubated with CM from H34 or UCH cells for the time indicated. ***B***, Effects of YON and 81027 CM. CM was applied to H11 cells for 12 h. ***C***, Effects of neutralizing antibodies. UCH CM was incubated with each neutralizing antibody (2 μg/ml) at 37°C for 1 h before application to H11 cells. ***D***, Time-dependent induction of MxA expression in Transwell cultures. H11 cells were seeded in the lower chamber, and H34 or UCH cells were seeded in the upper chamber. ***E***, Expression of MxA by NPC cells. H11, UCH, and 81027 cells were subjected to anti-MxA Western blotting or immunofluorescence. The images were obtained with confocal microscopy. Shown are the representative results, which were reproduced at least twice.

Activation of STATs by IFN-β and IL-6 in NPC cell CM

Both IFN-β and IL-6 activate STATs, which have six subtypes. The three response elements, IFN-stimulated response element (ISRE), STAT3, and γ-activated site (GAS) are the targets of STAT-1/2 heterodimer, STAT-3 homodimer, and STAT-1 homodimer, respectively (Ihle, 1996). By using reporter gene assays in HepG2 cells, we examined whether (1) IFN-β and IL-6 secreted by NPC cells were biologically active, (2) there were any other cytokines that could activate STATs, and (3) there were any substances that could induce secretion of IFN-β or IL-6.

In control experiments, recombinant IFN-α activated ISRE, IFN-β and IFN-γ activated ISRE and GAS, IL-6 activated STAT3 and GAS, and IL-8 had no effect, as expected from their specificity (Schindler, 1999) (Fig. 2*A*). None of the other cytokines detected in CM (IL-17, TNFα, TGFβ, and three CSFs) at 10 ng/ml activated any of these response elements (data not shown). UCH CM, but not H34 CM, activated all of the three response elements (Fig. 2*B*). For absorption experiments, UCH CM was incubated with neutralizing antibodies for 1 h before application. An antibody against IFN-β abolished its effect on ISRE, whereas those against IL-6 or IL-6 receptor abolished its effects on STAT3 and GAS. Antibodies against IFN-α or IFN-γ failed to neutralize the activities (Fig. 2*C*). These findings indicated that both IFN-β and IL-6 in UCH CM were biologically active, and that it contained no other cytokine that could activate STATs. The same results were reproduced when antibodies against IFN-β or IL-6 were precipitated with protein A-Sepharose after the 1 h incubation (data not shown), suggesting that UCH CM contained no substance that could induce secretion of IFN-β or IL-6.

As an alternative method to access the activity of the cytokines, we examined whether UCH CM could induce expression of MxA in control cells. *MxA* is one of the representative ISRE-driven genes (Der et al., 1998), encoding a dynamin family GTPase required for lipid transport in the smooth endoplasmic reticulum (Accola et al., 2002). Application of UCH CM induced expression of MxA in H11 cells (Fig. 3*A*). This activity was not contained in CM of H34 cells but was present in CM of another NPC1 cell line (YON) as well as 81027 cells (Fig. 3*B*). Consistent with the role of ISRE in MxA expression, a neutralizing antibody against IFN-β partially absorbed the activity of UCH CM and this effect was not observed with any of the antibodies against IFN-α, IFN-γ, IL-6, and IL-6 receptor (Fig. 3*C*).

To examine whether the similar activity was present in ordinary serum-containing medium, we used Transwell cultures in which cells were separated by a 0.22 μm pore filter. MxA was expressed by H11 cells when they were cocultured with UCH cells (Fig. 3*D*). We then examined whether NPC cells expressed MxA and found a dramatic increase of this protein both in UCH and 81027 cells. Anti-MxA immunofluorescence revealed its presence

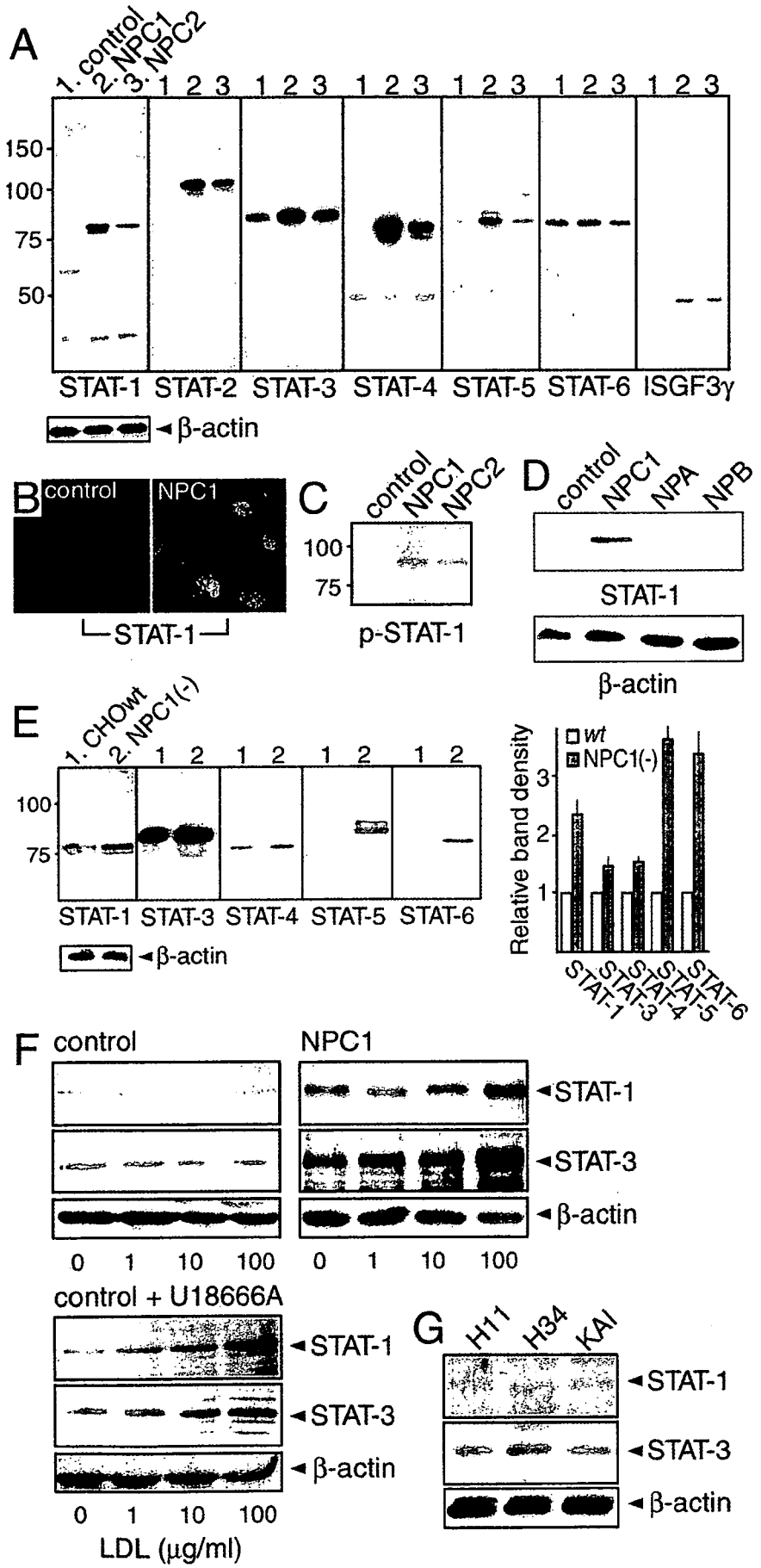

in the endoplasmic reticulum where it is normally localized (Accola et al., 2002), consistent with increased expression of the protein (Fig. 3*E*). These findings suggested that NPC cells cultured in normal serum-containing medium also secreted IFN-β and that this cytokine could act in both autocrine and paracrine manner.

Increases of STATs in NPC cells

Chronic secretion of inflammatory cytokines occurs in various disease states such as rheumatoid arthritis. This leads to increased protein levels of STATs in target cells and tissues, which serve as a marker of inflammation (Ivashkiv and Hu, 2003; Walker et al., 2006). Therefore, we examined the levels of STATs in NPC cells.

Western blotting showed that both UCH and 81027 cells contained increased levels of STAT-1 to -5 compared with H11 cells. Similarly, ISGF3γ, a protein that forms a complex with STAT-1 and -2 (Martinez-Moczygemba et al., 1997), was detectable in NPC cells, but not in H11 cells (Fig. 4*A*). In UCH cells, some of the STAT-1 protein was in its active state, because it was localized in the nucleus (Fig. 4*B*) and some of the protein was tyrosine phosphorylated (Fig. 4*C*).

To see whether the increase of STATs was specific for NPC, we examined their levels in NPA and NPB cells, and found no increase of STAT-1 (Fig. 4*D*) or other STATs (data not shown). To determine whether the increase was a common feature of NPC cells, levels in NPC1-deficient CHO cells were examined (Sugimoto et al., 2001). Similar to human NPC cells, NPC1-deficient CHO cells expressed increased levels of STAT-1, -3, -4, and -5. In

←

Figure 4. Levels of STATs in NPC cells. ***A***, ***C***, ***D***, Levels of STATs and ISGF3γ in human fibroblasts. Proteins in 1% Triton X-100 extracts were detected by Western blotting with indicated antibodies. Cells were from a control subject (H11) and patients with NPC1 mutations (UCH), NPC2 mutations (81027), NPA (GM0112), and NPB (GM0252). A total of 10 μg of protein was loaded in each lane. Molecular weights are given on the left (in kilodaltons). ***B***, STAT-1 immunofluorescence observed by confocal microscopy. ***E***, Levels of STATs in NPC1-deficient CHO cells [NPC1(−) cells]. Signal intensity of the bands was normalized to that of β-actin, and the intensity in NPC1(−) cells was expressed as relative to that in *wt* cells. Each bar represents the mean ± SEM of three determinations. ***F***, Effects of U18666A and LDL loading on STAT-1/STAT-3 levels. H34 and UCH cells were cultured in lipoprotein-deficient serum for 3 d, and then loaded with increasing concentrations of LDL for 24 h (top panels). In a separate set of H34 cells, they were loaded with LDL in the presence of 2 μg/ml U18666A (bottom panels). ***G***, Levels of STAT-1/STAT-3 in KAI cells. Shown are the representative results, which were reproduced at least twice.

these cells, the level of STAT-6 was also increased. The increase of STAT-3 and -4 was less clear than in human cells, but densitometric blot analysis showed a ~50% increase in signal intensity (Fig. 4*E*). This increase was not observed in "knock-in" cells that expressed human NPC1 (data not shown). No STAT-2 protein was detectable in CHO cell extracts, most likely because the antibody did not recognize the hamster protein. These findings suggested that the increase of STATs was a common and specific feature of NPC cells.

We also examined whether a similar increase of STATs was induced in control cells treated with 3β-[2-(diethylamino)ethoxy]-androst-5-en-17-one monohydrochloride (U18666A), which induces an NPC phenotype (Ko et al., 2001). Low-density lipoprotein (LDL) loading of cholesterol-depleted UCH cells caused a dose-dependent increase of STAT-1 and -3, but not in H11 cells. When H11 cells were loaded with LDL in the presence of U18666A, however, STAT levels increased in a dose-dependent manner (Fig. 4*F*). Thus, the increase of STATs could be induced in normal cells by U18666A treatment.

This observed increase of STATs in NPC cells was most likely attributable to autocrine effects of IFN-β and IL-6. In support of this notion, we found no increase in the levels of STAT-1 and STAT-3 in KAI cells (Fig. 4*G*).

Endosomal accumulation of TLR4 in NPC cells

We next investigated the biochemical basis for increased secretion of cytokines by NPC cells. Results from reporter gene assays in HepG2 cells (Fig. 2) and MxA induction experiments in H11 cells (Fig. 3) indicated that there was no activity in NPC cell CM that could induce secretion of IFN-β or IL-6, suggesting that their secretion was caused by some other intracellular event. NPC cells are characterized by aberrant endosomal membrane flow and it is possible that the activity of any signaling molecule in the endosomal compartment is altered.

We hypothesized that their secretion was attributable to activation of TLR4. TLRs are a family of receptor proteins that play a crucial role in innate immune responses. There are currently 11 known members of TLRs. TLR4 is selectively activated by bacterial LPS, and its activation by LPS requires an accessory protein MD-2 (Akashi et al., 2000). Our hypothesis was based on following observations. First, TLR4 activates transcription factors interferon regulatory factor-3 (IRF-3) and NFκB, which leads to production of IFN-β, IL-6, and IL-8 (Akira and Takeda, 2004), the same set of cytokines with elevated secretion in NPC cells. Second, TLR4 is localized both on the cell surface and endosome. It can be active on the endosome and its proper sorting to the lysosome is required to turn off its activity (Blander and Medzhitov, 2004; Doyle et al., 2004; Guillot et al., 2004; Husebye et al., 2006). Third, TLR4 is localized in raft microdomains and its activity can be modulated by the levels of cellular cholesterol (Triantafilou et al., 2002; Olsson and Sundler, 2006). To test our hypothesis, we examined whether (1) there were any alterations in the protein level and/or intracellular localization of TLR4, (2) siRNA against TLR4 could suppress cytokine secretion, and (3) U18666A could alter cellular responses to LPS.

Western blotting showed that UCH, YON, and 81027 cells contained markedly increased levels of TLR4. TLR4 was also detectable in 1% Triton X-100-insoluble fractions of NPC cells, suggesting its association with raft microdomains. As above, the cells from an adult-onset patient KAI proved to be the exception, because TLR4 was only marginally increased in cell extracts and was not detectable in 1% Triton X-100-insoluble fractions (Fig. 5*A*).

Because endogenous TLR4 could not be detected by immu-

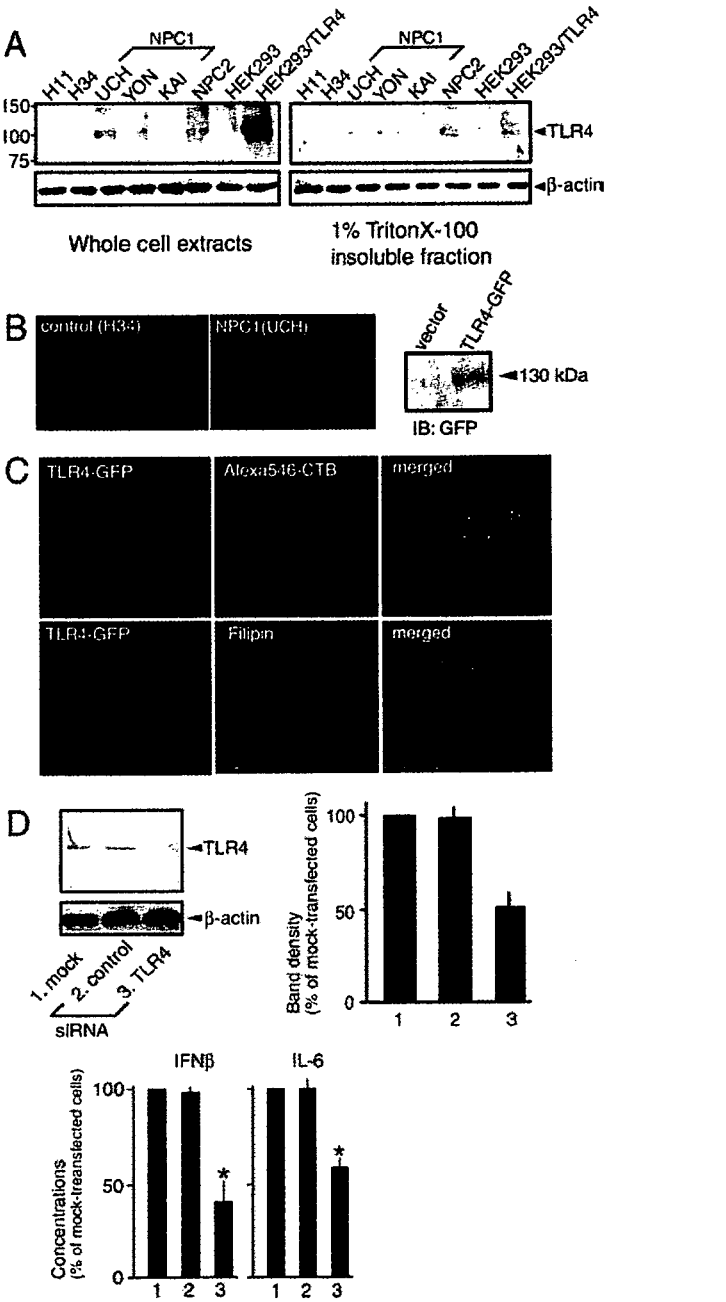

Figure 5. Levels of TLR4 and intracellular localization of TLR4-GFP in human NPC fibroblasts. ***A***, Levels of TLR4. Whole-cell extracts were prepared in 1% Triton X-100/0.2% SDS. The 1% Triton X-100-insoluble fractions were prepared as described in Materials and Methods. Extracts from native HEK293 cells and HEK293 cells expressing TLR4 were included. Molecular weights are given on the left (in kilodaltons). ***B***, ***C***, Intracellular localization of TLR4-GFP. In ***B***, TLR4-GFP was expressed in H34 or UCH cells. Shown on the right is an anti-GFP Western blot of H34 cell extracts transfected with vector or TLR4-GFP construct. In ***C***, 24 h after transfection with TLR4-GFP construct, UCH cells were exposed to Alexa 546-conjugated cholera toxin B subunit (CTB) before fixation (top panels) or fixed and stained with filipin (bottom panels). Images were obtained by confocal microscopy. In ***A–C***, shown are the representative results, which were reproduced at least twice. ***D***, Effects of TLR4 siRNA. siRNA was introduced to UCH cells by electroporation, and at 48 h after electroporation, whole-cell extracts were processed for Western blotting or the cells were further incubated for 24 h in serum-free DMEM for preparation of CM. Signal intensity of the bands was normalized to that of β-actin, and the intensity in siRNA-transfected cells was expressed as relative to that in mock-transfected cells. Each bar represents the mean ± SEM of three determinations. Because absolute values varied between experiments, concentrations of IFN-β and IL-6 were also expressed as relative to the values of mock-transfected cells. Each bar represents the mean ± SEM of three determinations, each performed in duplicate. *$p < 0.01$, significantly different from the values of mock-transfected cells.

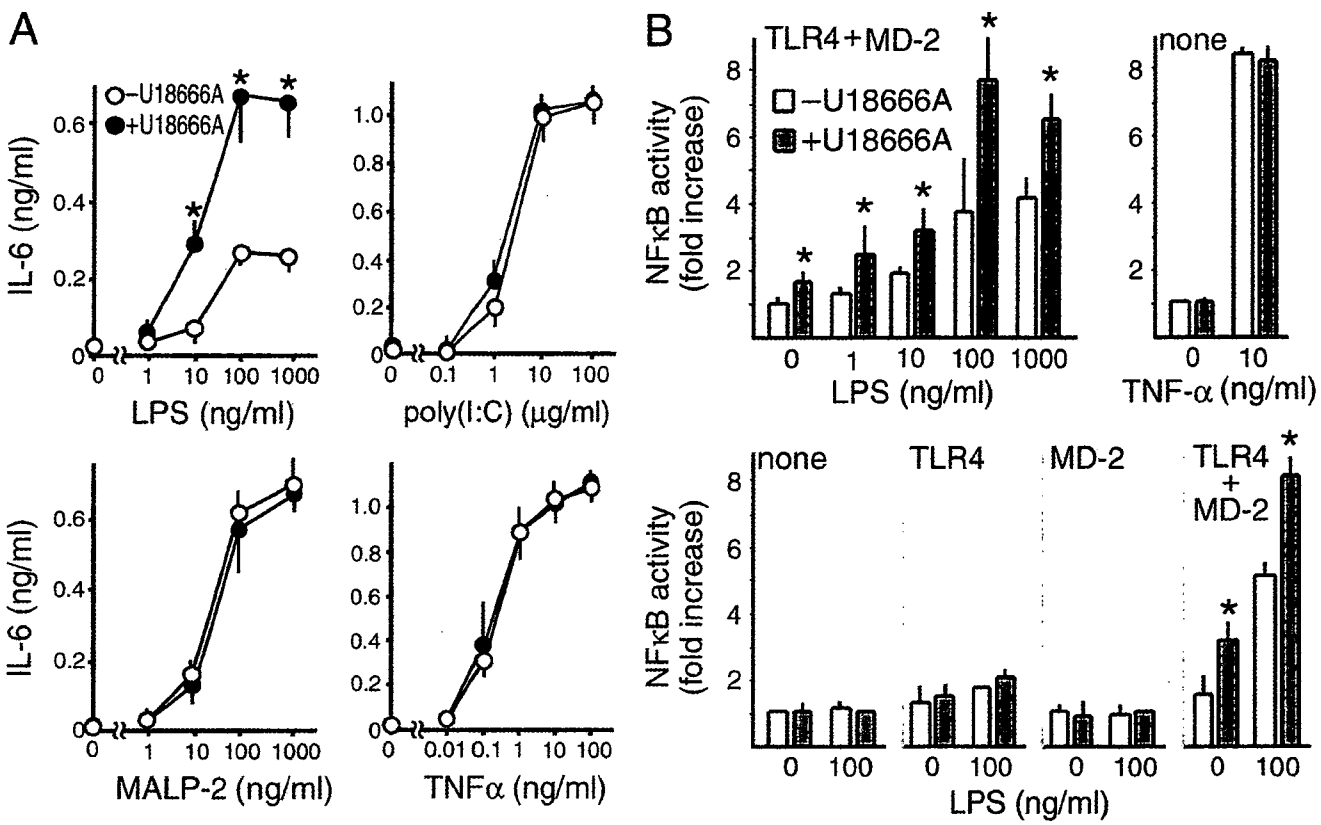

Figure 6. Effects of U18666A on cellular responses to LPS. ***A***, IL-6 secretion by H34 control cells. Cells were incubated with or without U18666A (2 μg/ml) for 16 h and further incubated for 12 h in serum-free DMEM containing LPS, poly(I:C), MALP-2, or TNFα. Concentrations of IL-6 in the medium were determined by ELISA. Each point represents the mean ± SEM of three determinations each performed in duplicate. ***B***, NFκB reporter gene assay. HEK293 cells were transfected with NFκB luciferase construct together with expression plasmids for TLR4 and/or MD-2 as indicated. At 24 h after transfection, they were stimulated with LPS or TNFα for 6 h in the absence or presence of U18666A (2 μg/ml). Each bar represents the mean ± SEM of three determinations, each performed in triplicate. *$p < 0.01$, significantly different from the values in the absence of U18666A.

nocytochemistry, we determined the intracellular localization of a TLR4-GFP fusion protein, which has been shown to behave similar to the endogenous protein (Latz et al., 2002). In H34 cells, TLR4-GFP was located both on the cell surface and in tiny vesicles that were diffusely distributed throughout the cytoplasm. In contrast, in UCH cells, it was predominantly found in perinuclear vesicles (Fig. 5*B*). In NPC cells, ganglioside GM1 accumulates in the early endosome, whereas cholesterol accumulates in the late endosome and lysosome (Sugimoto et al., 2001). Intracellular vesicles that contained TLR4-GFP did not incorporate Alexa 546-conjugated cholera toxin B subunit, but were stained with filipin, suggesting the accumulation of TLR4-GFP in cholesterol-enriched late endosomes/lysosomes (Fig. 5*C*).

siRNA was introduced into UCH cells by electroporation. TLR4 siRNA decreased the level of this protein in cell extracts, and also caused significant reductions in IFN-β and IL-6 in CM (Fig. 5*D*). Similar results were obtained with 81027 cells (data not shown).

The response of H34 cells to LPS was assessed by quantification of secreted IL-6. LPS caused dose-dependent secretion of IL-6 by H34 cells. When cells were pretreated with U18666A, the amounts of secreted IL-6 were significantly increased. In these experiments, we also examined the cellular response to poly(I:C), MALP-2, and TNFα, all of which can activate NFκB. Poly(I:C) is a selective ligand for TLR3 (Akira and Takeda, 2004). Similar to TLR4, TLR3 activates both IRF-3 and NFκB and is located in endosomal compartments (de Bouteiller et al., 2005). However, unlike TLR4, it has never been demonstrated that this receptor is associated with raft microdomains or that the levels of cellular cholesterol influence its function. Similar to LPS, MALP-2 is a lipoprotein; however, it is a selective ligand for TLR2 and -6 (Akira and Takeda, 2004), whereas TNFα is not a ligand for TLRs. U18666A caused no significant changes in the cellular responses to these ligands (Fig. 6*A*).

LPS has multiple effects and some of them are independent from TLR4. To confirm the effect of U18666A on TLR4, we used an NFκB reporter gene assay in HEK293 cells, which do not express TLR4 or MD-2 (Fig. 6*B*). When cells were transfected with TLR4 and MD-2 constructs, LPS caused a dose-dependent activation of the reporter, and its effect was significantly enhanced in the presence of U18666A. Unexpectedly, we found that U18666A alone caused activation of the reporter in the presence of TLR4/MD-2, and was effective only when both TLR4 and MD-2 were expressed. The effect of TNFα was not affected by U18666A, confirming the specificity of this effect for TLR4/MD-2. Using this reporter gene assay, we detected no effect of UCH CM regardless of expression of TLR4/MD-2 (data not shown), consistent with the lack of activity in NPC cell CM to induce cytokine secretion.

Expression of STATs, TLR4, and IL-6 in the NPC mouse brain

The above findings in cultured NPC fibroblasts suggested that secretion of cytokines leads to activation of STATs and that this secretion is attributable, at least in part, to the endosomal accumulation of TLR4. To explore the role of these molecules in NPC pathogenesis, we first examined the protein levels and cellular

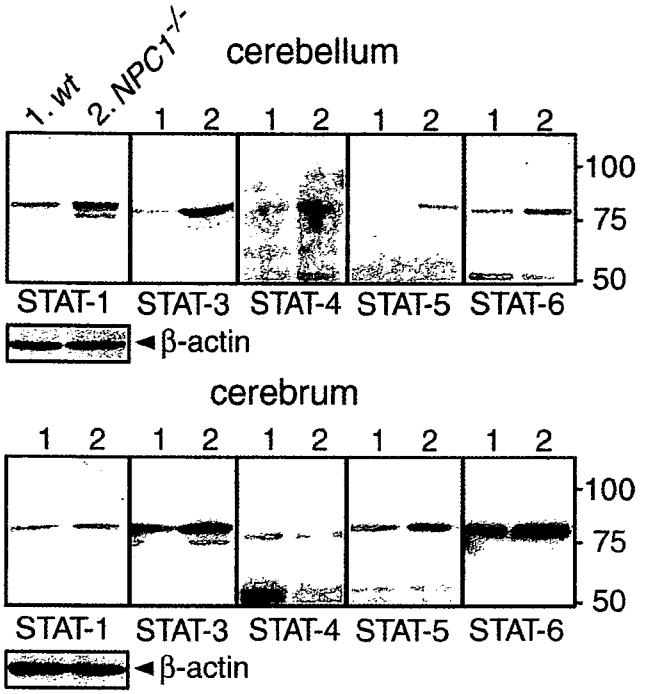

Figure 7. Levels of STATs in the NPC mouse brain. Brain extracts were obtained from 6-week-old $NPC1^{+/+}$ (*wt*) and $NPC1^{-/-}$ littermates and analyzed by Western blotting. A total of 10 μg of protein was loaded in each lane. Molecular weights are given on the right (in kilodaltons). Shown are the representative results, which were reproduced at least twice.

localization of STATs in the NPC mouse brain, using tissues from 6-week-old *wt* and $NPC1^{-/-}$ littermates.

Western blotting of cerebral and cerebellar extracts revealed a clear increase of STAT-3 and -6 and a marginal increase of STAT-1, -4, and -5 in $NPC1^{-/-}$ mice compared with *wt* mice (Fig. 7). The profile of the increased STATs was different from that observed in cultured human fibroblasts because STAT-3 was increased most prominently. STAT-2 was undetectable, most likely because the antibody did not recognize the mouse protein. We then examined the cellular origins of STAT-1, -3, and -6 by immunohistochemistry of cerebellar sections.

In the following analysis, activated astroglial and microglial cells were detected with antibodies against GFAP and MAC1, respectively. Glial cell activation in the NPC mouse brain is a progressive process, and in the cerebellar cortex of 6-week-old mice, both GFAP-positive and MAC1-positive cells can be seen in every layer. There is, however, a regional difference in their abundance: GFAP-positive astroglial cells are most abundant in the granule cell layer, whereas MAC1-positive microglial cells are most abundant in the white matter. These glial cells contained undetectable levels of immunoreactivity for PCNA (data not shown), suggesting that they are not actively proliferating.

In *wt* sections, STAT-1 immunoreactivity was observed in Purkinje and granule cell layers. Immunoreactivity in these regions was increased and signal was also observed in the molecular cell layer of the $NPC1^{-/-}$ cerebellum (Fig. 8*A*). Double immunofluorescence analysis did not reveal any colocalization of STAT-1 with either GFAP or MAC1 (data not shown). In *wt* sections, STAT-3 immunoreactivity was observed in molecular and Purkinje cell layers. Immunoreactivity was increased in $NPC1^{-/-}$ cerebellum, and strong signal was also observed in the granule cell layer (Fig. 8*B*). STAT-3 immunoreactivity colocalized with both GFAP and MAC1 as shown in the representative images of the granule cell layer and the white matter, respectively (Fig. 8*C*). STAT-6 immunoreactivity was not observed in neuronal or glial cells (data not shown) but was confined to vascular endothelial cells, and it appeared to be increased in $NPC1^{-/-}$ sections (Fig. 8*D*). These findings suggested that, in the $NPC1^{-/-}$ mouse cerebellum, STAT-1 was expressed by neuronal cells, STAT-3 by both neuronal and glial cells, and STAT-6 by endothelial cells. Similar results were obtained using immunohistochemical analysis of cerebral sections (data not shown).

Next, we examined cellular localization of TLR4 and IL-6. We focused on IL-6 in the subsequent histochemical analysis and genetic deletion experiments because of the prominent increase of STAT-3 and its expression by both neuronal and glial cells. TLR4 immunoreactivity was barely detectable in *wt* cerebellar sections, whereas clear signal was observed in cells localized in the granule cell layer and the white matter of $NPC1^{-/-}$ sections (Fig. 9*A*). Double immunofluorescence labeling showed colocalization of TLR4 with both GFAP and MAC1 as shown in the representative images of the granule cell layer and the white matter, respectively (Fig. 9*B*). Similarly, IL-6 immunoreactivity was barely detectable in *wt* sections (data not shown), but in $NPC1^{-/-}$ sections, a clear colocalization with GFAP and MAC1 was observed (Fig. 9*C*). These findings suggested that, in the $NPC1^{-/-}$ mouse cerebellum, TLR4 and IL-6 are expressed by glial cells, but not by neuronal cells.

Genetic deletion of TLR4 reduced cellular IL-6 secretion

To confirm the role of TLR4 in IL-6 secretion, we generated double gene knock-out mice that lacked NPC1 and TLR4. IL-6 secretion was examined in fibroblasts obtained from 6-week-old littermates with different TLR4 genotypes (Fig. 10, left panel). As expected, $NPC1^{-/-}/TLR4^{+/+}$ fibroblasts secreted high levels of IL-6. Its concentration was marginally reduced in $NPC1^{-/-}/TLR4^{+/-}$ cells and was reduced to ~30% in $NPC1^{-/-}/TLR4^{-/-}$ cells. These results confirmed the role of TLR4 in IL-6 secretion by NPC fibroblasts, but also suggested the presence of other factors responsible for the residual secretion of IL-6.

Despite this reduction of IL-6 secretion by fibroblasts, Western blotting and immunohistochemistry revealed that both STAT levels and the number of activated glial cells were indistinguishable between $NPC1^{-/-}/TLR4^{+/+}$ and $NPC1^{-/-}/TLR4^{-/-}$ mice (data not shown). In addition, the lifespan of the $NPC1^{-/-}/TLR4^{-/-}$ mice was not significantly different from that of $NPC1^{-/-}/TLR4^{+/+}$ mice (data not shown). Assuming that IL-6 expression by glial cells is also decreased in the double gene knock-out mice, these negative findings argue against a role of TLR4 and IL-6 in NPC pathogenesis. However, it is possible that residual IL-6, which might also be secreted by glial cells, is sufficient to induce pathological changes. To address this question, we generated double gene knock-out mice that lacked NPC1 and IL-6.

Genetic deletion of IL-6 normalized STAT levels, suppressed glial cell activation, and prolonged the life span of NPC mice.

IL-6 secretion was again assessed in fibroblasts with different IL-6 genotypes. As expected, $NPC1^{-/-}/IL\text{-}6^{+/+}$ cells secreted a high concentration of IL-6. Its concentration in $NPC1^{-/-}/IL\text{-}6^{+/-}$ cells was about one-half of that found in $NPC1^{-/-}/IL\text{-}6^{+/+}$ cells, and it was undetectable in $NPC1^{-/-}/IL\text{-}6^{-/-}$ cells (Fig. 10, right panel).

Genetic deletion of IL-6 caused obvious alterations in STAT levels and brain pathology. Western blotting of brain extracts from 6-week-old littermates showed that $NPC1^{-/-}/IL\text{-}6^{+/+}$ mice

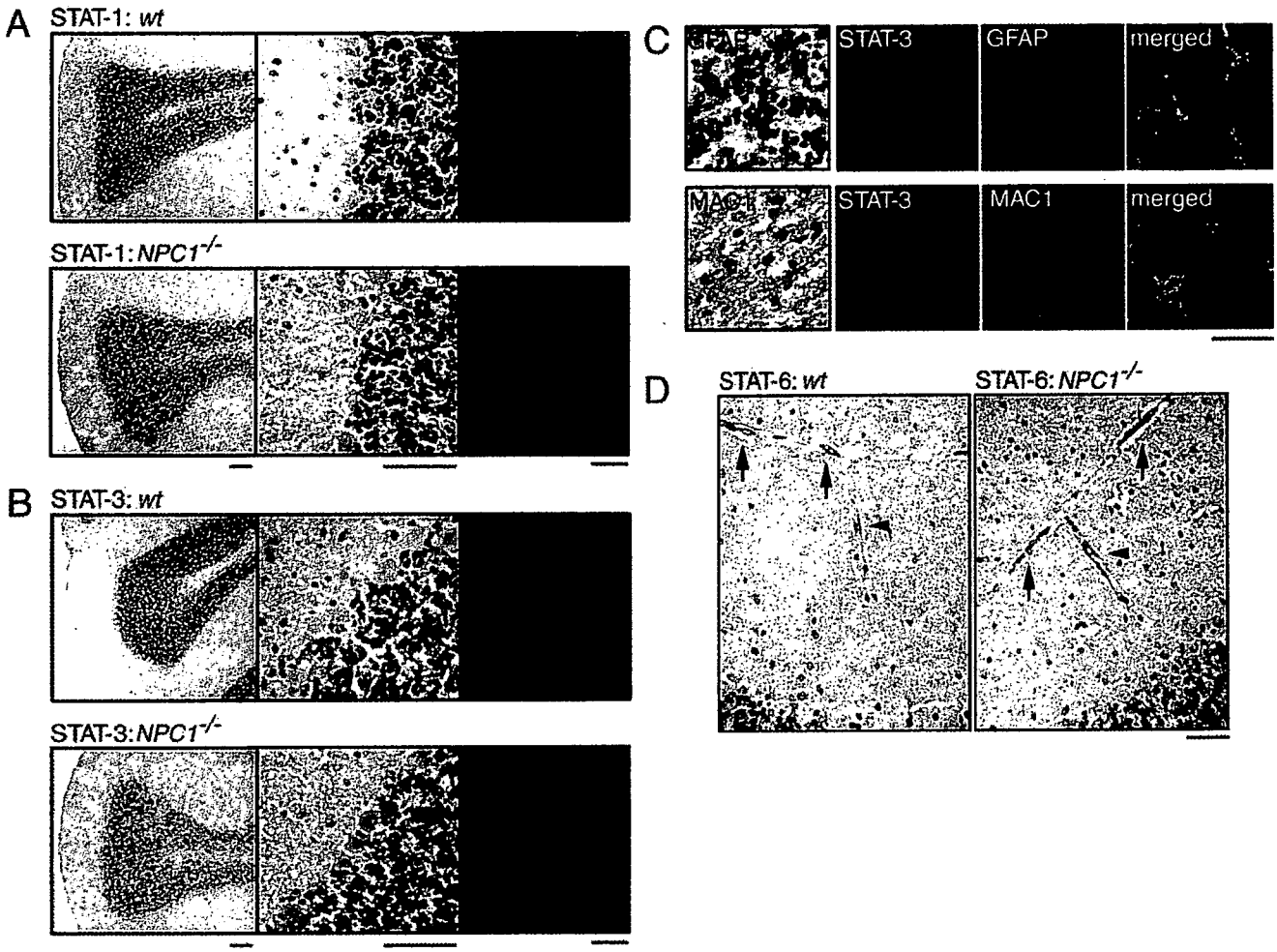

Figure 8. Cellular localizations of STATs in the NPC mouse cerebellum. Brain sections were obtained from 6-week-old littermates. ***A***, ***B***, STAT-1/STAT-3 immunostaining. Cerebellar sections were stained with indicated antibodies, and bound antibodies were detected by HRP-conjugated secondary antibody and visualized with DAB or by Alexa 488-conjugated secondary antibody followed by confocal imaging. Scale bars, 100 μm. ***C***, Double immunofluorescence of $NPC1^{-/-}$ sections with STAT-3 and GFAP or MAC1. Images are from the granule cell layer (GFAP) or the white matter (MAC1). Bound antibodies were detected by Alexa 488- or Alexa 568-conjugated secondary antibodies. In the left panels, bound antibodies were detected by HRP-conjugated secondary antibody and visualized with DAB. Scale bar, 20 μm. ***D***, STAT-6 immunostaining of blood vessels in the subarachnoid space (arrows) and the molecular cell layer (arrowheads). Scale bar, 100 μm. Shown are the representative results, which were reproduced at least twice.

had increased amounts of STATs, compared with $NPC1^{+/+}$/IL-$6^{+/+}$ mice. The levels detected in $NPC1^{-/-}$/IL-$6^{+/-}$ mice were comparable with those found in $NPC1^{-/-}$/IL-$6^{+/+}$ mice, whereas the levels in $NPC1^{-/-}$/IL-$6^{-/-}$ mice were significantly decreased. The exception was STAT-6 that did not change significantly between IL-6 genotypes (Fig. 11*A*). In agreement with the Western blot analysis, STAT-3 immunoreactivity in Purkinje and molecular cell layers was decreased in $NPC1^{-/-}$/IL-$6^{-/-}$ mice compared with $NPC1^{-/-}$/IL-$6^{+/+}$ or $NPC1^{-/-}$/IL-$6^{+/-}$ mice (Fig. 11*B*).

We found that the number of activated glial cells was markedly decreased in $NPC1^{-/-}$/IL-$6^{-/-}$ mice. The decrease of GFAP-positive astroglial cells was most apparent in the granule cell layer and the thalamic nuclei in sections from 6-week-old littermates (Fig. 11*C*). A similar decrease was also seen in sections from 3- and 9-week-old mice (data not shown). Accordingly, Western blotting demonstrated reduced levels of GFAP in the $NPC1^{-/-}$/IL-$6^{-/-}$ brain (Fig. 11*A*). Similar to astroglial cells, the number of MAC1-positive microglial cells was decreased in $NPC1^{-/-}$/IL-$6^{-/-}$ mice (Fig. 11*D*). Despite this reduction of activated glial cells, we could not see appreciable differences in the number of Purkinje cells between different genotypes (data not shown). The lifespan of $NPC1^{-/-}$/IL-$6^{-/-}$ mice, but not that of $NPC1^{-/-}$/IL-$6^{+/-}$ mice, was modestly increased compared with $NPC1^{-/-}$/IL-$6^{+/+}$ mice (Table 2).

Discussion

The main cellular phenotype of NPC is aberrant endosomal membrane trafficking, which leads to an accumulation of cholesterol and other lipids in the endosomal/lysosomal compartment. The fundamental question in NPC pathogenesis is how this impairment of membrane flow causes pathological changes including neuronal cell loss and glial cell activation. In the current study, we presented evidence that TLR4, IL-6, and STATs constitute a potential link between impaired membrane flow and glial cell activation.

Our findings in cultured NPC fibroblasts indicate that secretion of the cytokines is attributable, at least in part, to the endosomal accumulation of TLR4. TLR4 is peculiar among the TLRs in that it can be located in endosomal compartments (Guillot et al., 2004; Husebye et al., 2006) and associates with cholesterol-enriched raft microdomains (Triantafilou et al., 2002; Olsson and

Sundler, 2006). These features of TLR4 may underlie its accumulation, because NPC cells accumulate raft microdomains in their endosomes (Lusa et al., 2001). In the NFκB reporter gene assay using HEK293 cells, U18666A alone could activate NFκB in cells expressing TLR4 and MD-2, and NPC cell CM contained no activity to stimulate this receptor. These findings suggest that, in NPC cells, activation of TLR4 is caused by the endosomal accumulation in itself, and hence is a direct consequence of impaired membrane flow. This is consistent with previous findings that TLR4 could be activated by antibody-mediated aggregation in the absence of any ligand (Visintin et al., 2003) and that its proper sorting from the endosome to the lysosome was required to turn off its activity (Husebye et al., 2006). Because TLR4 triggers multiple signaling events that activate intracellular membrane trafficking (Blander and Medzhitov, 2004; Doyle et al., 2004), its activation in NPC cells may represent one of the adaptive responses of the cells to resume membrane trafficking.

Genetic deletion of TLR4 in NPC mice reduced IL-6 secretion by primary cultured fibroblasts, confirming the role of TLR4 in IL-6 secretion by these cells. Immunohistochemical analysis revealed expression of TLR4, IL-6, and STAT-3 by glial cells in the NPC mouse cerebellum, suggesting that TLR4 and downstream signaling events are also activated in glial cells *in vivo*. Direct evidence for the role of TLR4 in IL-6 expression by glial cells, however, is lacking. Furthermore, the negative effects of genetic deletion of TLR4 on STAT levels and glial cell activation indicate that, even if this receptor is responsible for IL-6 expression, the contribution is only partial and there must be other factors responsible for the expression. Additional analysis will be required to identify these factors and to verify the role of TLR4 in IL-6 expression by glial cells, such as other members of the TLR family, which have been shown to be expressed by glial cells (Kielian, 2006).

Selective expression of IL-6 and STATs by specific cell types in the *NPC1*$^{-/-}$ mouse cerebellum and the effects of genetic deletion of IL-6 indicate that this cytokine plays multiple roles in NPC pathogenesis, acting in both autocrine and paracrine manner. The autocrine effect is evident by expression of IL-6 and STAT-3 by glial cells and suppression of their activation in the absence of IL-6. Because this cytokine has been shown to be involved in glial cell activation that occurs secondarily to neuronal damage (Penkowa et al., 2001; Cardenas and Bolin, 2003), our findings do not exclude the occurrence of glial cell activation triggered by neuronal damage in the *NPC1*$^{-/-}$ brain. However, given the expression of TLR4, our data suggest that glial cell activation in the *NPC1*$^{-/-}$ mouse brain may occur in a cell-autonomous manner. The paracrine effect is evident by increased expression of STAT-1 and -3 by Purkinje

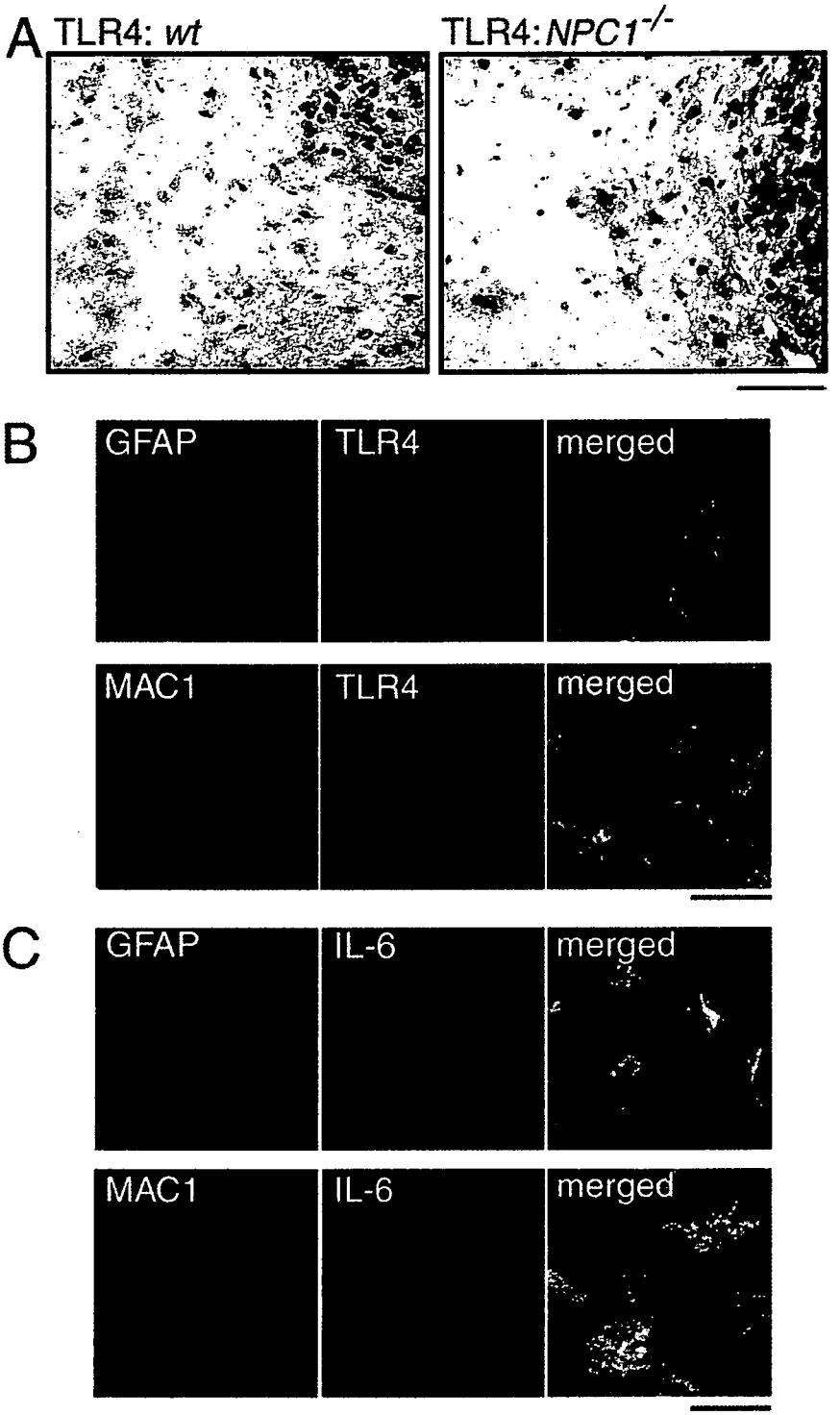

Figure 9. Cellular localizations of TLR4 and IL-6 in the NPC mouse cerebellum. Brain sections were obtained from 6-week-old littermates. ***A***, TLR4 immunostaining. Scale bar, 100 μm. ***B***, ***C***, Double immunofluorescence of *NPC1*$^{-/-}$ sections with TLR4 or IL-6 and GFAP or MAC1. Images are from the granule cell layer (GFAP) or the white matter (MAC1). Scale bars, 20 μm. Shown are the representative results, which were reproduced at least twice.

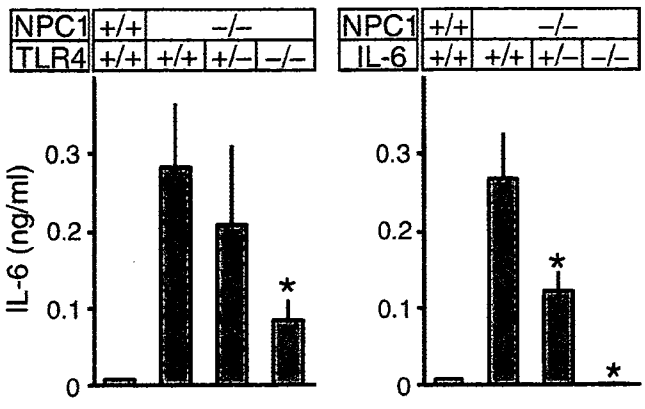

Figure 10. Effects of genetic deletion of TLR4 or IL-6 on IL-6 secretion by primary cultured skin fibroblasts. Cells were obtained from 6-week-old littermates with individual genotypes. Each bar represents the mean ± SEM of three determinations, each performed in duplicate. *$p < 0.01$, significantly different from the values of $NPC1^{-/-}/TLR4^{+/+}$ cells (left) or $NPC1^{-/-}/IL\text{-}6^{+/+}$ cells (right).

Table 2. Effects of genetic deletion of IL-6 on the lifespan of $NPC1^{-/-}$ mice

Background	IL-6	Male	Female	Sum
BALB/c	+/+	68 ± 4.1 (25)	72 ± 4.2 (25)	70 ± 4.5 (50)
BALB/c × C57BL	+/+	70 ± 2.6 (7)	70 ± 7.2 (7)	70 ± 5.2 (14)
	+/−	69 ± 1.1 (13)	73 ± 5.6 (11)	71 ± 4.3 (24)
	−/−	77 ± 5.7*(6)	82 ± 6.7*(6)	80 ± 6.7*(12)

Values represent the mean ± SD. The number of animals in each group is given in parentheses.
*$p < 0.01$, significantly different from the values of $IL\text{-}6^{+/+}$ animals.

cells and its normalization in the absence of IL-6. This is the first experimental demonstration that Purkinje cells in the $NPC1^{-/-}$ mouse cerebellum are under the influence of a substance secreted by glial cells. Despite its drastic effect on glial cell activation, however, genetic deletion of IL-6 in $NPC1^{-/-}$ mice failed to cause appreciable changes in Purkinje cell survival, and caused only a modest increase (~11%) of their lifespan. These findings suggest a limited role of any substances secreted by glial cells in neurodegeneration, providing additional evidence for the notion that Purkinje cell death is a cell-autonomous event in these animals (Ko et al., 2005).

The roles of the other two cytokines, IFN-β and IL-8, in NPC pathogenesis remain to be investigated. The potential role of IFN-β, at least at the cellular level, is underscored by its activity to induce expression of MxA. Because MxA is a dynamin family GTPase involved in lipid transport (Accola et al., 2002), its increased expression may also represent one of the adaptive responses of the cells to resume membrane trafficking. Because IL-8 acts as a chemokine for inflammatory cells, it may also be implicated in glial cell activation in the NPC brain.

Our observations in double gene knock-out mice suggest that a benefit of an antiinflammatory therapy for NPC in this animal model is, at best, limited. This is consistent with the failure of minocycline, a drug that reduces IL-6 secretion (Zanjani et al.,

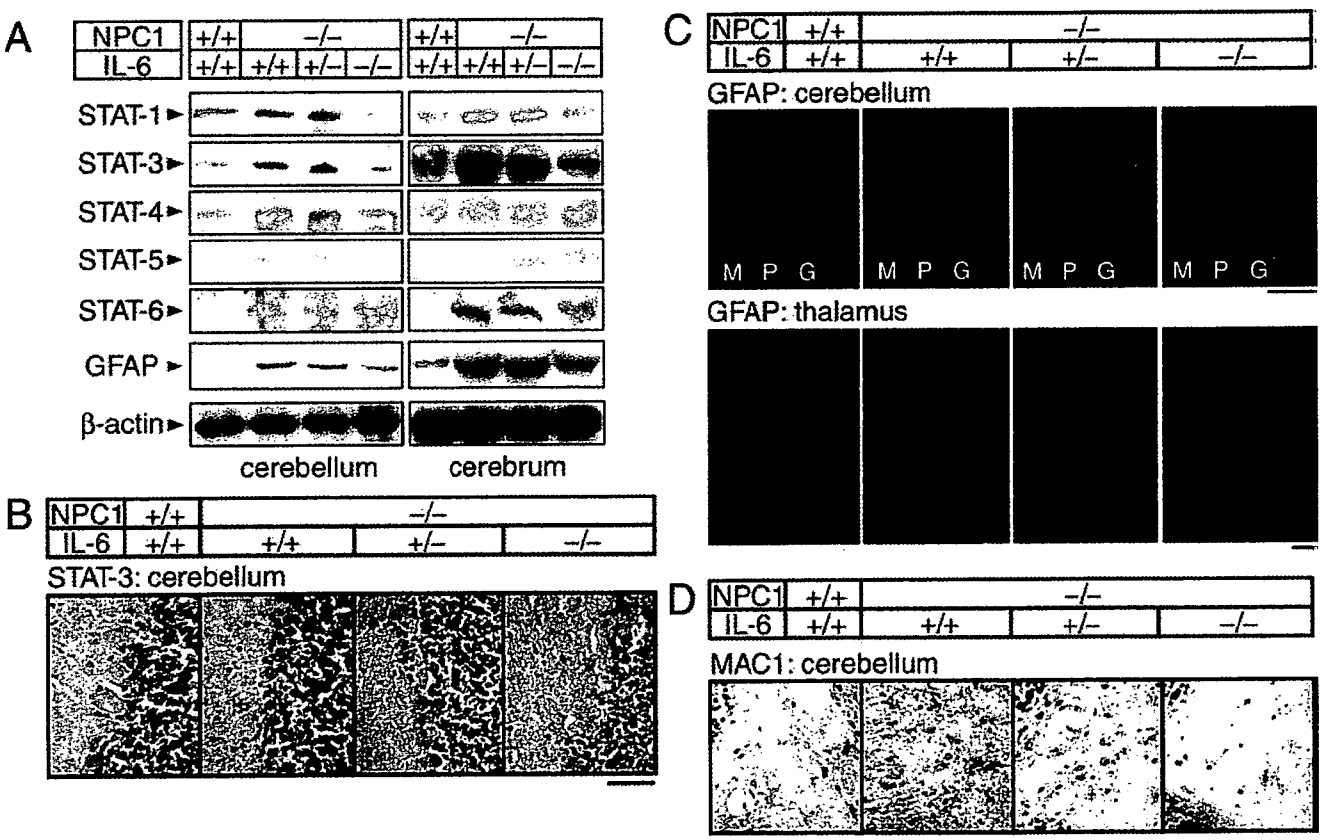

Figure 11. Effects of genetic deletion of IL-6 on STAT levels and glial cell activation in the NPC mouse brain. Brains were obtained from 6-week-old littermates with individual genotypes. ***A***, Levels of STATs and GFAP. Western blotting of 1% Triton X-100 extracts was performed as described in Figure 7. ***B***, STAT-3 immunostaining. Cerebellar sections were stained with anti-STAT-3 followed by HRP-conjugated secondary antibody. ***C***, GFAP immunostaining. Sections were stained with anti-GFAP followed by Alexa 488-conjugated secondary antibody. M, P, and G denote molecular, Purkinje, and granule cell layers, respectively. ***D***, MAC1 immunostaining. Cerebellar sections were stained with anti-MAC1 followed by HRP-conjugated secondary antibody. Shown are the representative images of the white matter. In ***A–D***, shown are the representative results, which were reproduced at least twice. Scale bars, 50 μm.

2006), to delay the onset of neurological symptoms in *NPC1*$^{-/-}$ mice (Erickson and Bernard, 2002). A potential benefit of such a therapy against the human disease, however, remains to be determined. This notion is supported by our findings on KAI cells, which expressed marginally increased levels of TLR4 and did not secrete IL-6. Most of the NPC patients die within the second decade of life. The patient KAI was atypical in that he manifested an adult-onset phenotype, with neurological symptoms at the age of 25 and eventual demise at the age of 42 (Yamamoto et al., 2000). The cause–effect relationship between the lack of IL-6 secretion and the mild clinical phenotype warrants additional examination.

Finally, TLR4 has been implicated in glial cell activation that occurs in other, more common neurodegenerative diseases including Alzheimer's disease (Kakimura et al., 2002). NPC and Alzheimer's disease share several pathological features including the formation of neurofibrillary tangles (Suzuki et al., 1995) and the accumulation of β-amyloid (Saito et al., 2002), suggesting the presence of common biochemical mechanisms involved in the pathogenesis of these two diseases. Activation of TLR4 and downstream signaling events may be one of the common biochemical mechanisms involved in glial cell activation that occurs in the brains of NPC and Alzheimer's disease.

References

Accola MA, Huang B, Masri AA, McNiven MA (2002) The antiviral dynamin family member, MxA, tublates lipids and localizes to the smooth endoplasmic reticulum. J Biol Chem 277:21829–21835.

Ahmad I, Lope-Piedrafita S, Bi X, Hicks C, Yao Y, Yu C, Chaitkin E, Howison CM, Weberg L, Trouard TP, Erickson RP (2005) Allopregnanolone treatment, both as a single injection or repetitively, delays demyelination and enhances survival of Niemann-Pick C mice. J Neurosci Res 82:811–821.

Akashi S, Shimazu R, Ogata H, Nagai Y, Takeda K, Kimoto M, Miyake K (2000) Cutting edge: cell surface expression and lipopolysaccharide signaling via the Toll-like receptor 4-MD-2 complex on mouse peritoneal macrophages. J Immunol 164:3471–3475.

Akira S, Takeda K (2004) Toll-like receptor signaling. Nat Rev Immunol 4:499–511.

Baudry M, Yao Y, Simmons D, Liu J, Bi X (2003) Postnatal development of inflammation in a murine model of Niemann-Pick type C disease: immunohistochemical observations of microglia and astroglia. Exp Neurol 184:887–903.

Bi X, Liu J, Yao Y, Baudry M, Lynch G (2005) Deregulation of the phosphatidylinositol-3 kinase signaling cascade is associated with neurodegeneration in npc1−/− mouse brain. Am J Pathol 167:1081–1092.

Blander JM, Medzhitov R (2004) Regulation of phagosome maturation by signals from Toll-like receptors. Science 304:1014–1018.

Cardenas H, Bolin LM (2003) Compromised reactive microgliosis in MPTP-lesioned IL-6 KO mice. Brain Res 985:89–97.

Carstea ED, Morris JA, Coleman KG, Loftus SK, Zhang D, Cummings C, Gu J, Rosenfeld MA, Pavan WJ, Krizman DB, Nagle J, Polymeropoulos MH, Sturley SL, Ioannou YA, Higgins ME, Comly M, Cooney A, Brown A, Kaneski CR, Blanchette-Mackie EJ, et al. (1997) Niemann-pick C1 disease gene: homology to mediators of cholesterol homeostasis. Science 277:228–231.

de Bouteiller O, Merck E, Hasan UA, Hubac S, Benguigui B, Trinchieri G, Bates EE, Caux C (2005) Recognition of double-stranded RNA by human Toll-like receptor 3 and downstream receptor signaling requires multimerization and an acidic pH. J Biol Chem 280:38133–38145.

Der SD, Zhou A, Williams BR, Silverman RH (1998) Identification of genes differentially regulated by interferon α, β, or γ using oligonucleotide arrays. Proc Natl Acad Sci USA 95:15623–15628.

Doyle SE, O'Connell RM, Miranda GA, Vaidya SA, Chow EK, Liu PT, Suzuki S, Suzuki N, Modlin RL, Yeh WC, Lane TF, Cheng G (2004) Toll-like receptors induce a phagocytic gene program through p38. J Exp Med 199:81–90.

Erickson RP, Bernard O (2002) Studies on neuronal death in the mouse model of Niemann-Pick C disease. J Neurosci Res 68:738–744.

German DC, Liang CL, Song T, Yazdani U, Xie C, Dietschy JM (2002) Neurodegeneration in the Niemann-Pick C mouse: glial involvement. Neuroscience 109:437–450.

Griffin LD, Gong W, Verot L, Mellon SH (2004) Niemann-Pick type C disease involves disrupted neurosteroidogenesis and responds to allopregnanolone. Nat Med 10:704–711.

Guillot L, Medjane S, Le-Barillec K, Balloy V, Danel C, Chignard M, Si-Tahar M (2004) Response of human pulmonary epithelial cells to lipopolysaccharide involves Toll-like receptor 4 (TLR4)-dependent signaling pathways: evidence for an intracellular compartmentalization of TLR4. J Biol Chem 279:2712–2718.

Higashi Y, Murayama S, Pentchev PG, Suzuki K (1993) Cerebellar degeneration in the Niemann-Pick type C mouse. Acta Neuropathol (Berl) 85:175–184.

Husebye H, Halaas O, Stenmark H, Tunheim G, Sandanger O, Bogen B, Brech A, Latz E, Espevik T (2006) Endocytic pathways regulate Toll-like receptor 4 signaling and link innate and adaptive immunity. EMBO J 25:683–692.

Ihle JN (1996) STATs: signal transducers and activators of transcription. Cell 84:331–334.

Ivashkiv LB, Hu X (2003) The JAK/STAT pathway in rheumatoid arthritis: pathogenic or protective? Arthritis Rheum 48:2092–2096.

Kakimura J, Kitamura Y, Takata K, Umeki M, Suzuki S, Shibagaki K, Taniguchi T, Nomura Y, Gebicke-Haerter PJ, Smith MA, Perry G, Shimohama S (2002) Microglial activation and amyloid-β clearance induced by exogenous heat-shock proteins. FASEB J 16:601–603.

Kielian T (2006) Toll-like receptors in central nervous system glial inflammation and homeostasis. J Neurosci Res 83:711–730.

Ko DC, Gordon MD, Jin JY, Scott MP (2001) Dynamic movements of organelles containing Niemann-Pick C1 protein: NPC1 involvement in late endocytic events. Mol Biol Cell 12:601–614.

Ko DC, Milenkovic L, Beier SM, Manuel H, Buchanan J, Scott MP (2005) Cell-autonomous death of cerebellar purkinje neurons with autophagy in Niemann-Pick type C disease. PLoS Genet 1:81–95.

Latz E, Visintin A, Lien E, Fitzgerald KA, Monks BG, Kurt-Jones EA, Golenbock DT, Espevik T (2002) Lipopolysaccharide rapidly traffics to and from the Golgi apparatus with the toll-like receptor 4-MD-2-CD14 complex in a process that is distinct from the initiation of signal transduction. J Biol Chem 277:47834–47843.

Loftus SK, Morris JA, Carstea ED, Gu JZ, Cummings C, Brown A, Ellison J, Ohno K, Rosenfeld MA, Tagle DA, Pentchev PG, Pavan WJ (1997) Murine model of Niemann-Pick C disease: mutation in a cholesterol homeostasis gene. Science 277:232–235.

Lusa S, Blom TS, Eskelinen EL, Kuismanen E, Mansson JE, Ikonen E (2001) Depletion of rafts in late endocytic membranes is controlled by NPC1-dependent recycling of cholesterol to the plasma membrane. J Cell Sci 114:1893–1900.

Martinez-Moczygemba M, Gutch MJ, French DL, Reich NC (1997) Distinct STAT structure promotes interaction of STAT2 with the p48 subunit of the interferon-α stimulated transcription factor ISGF3γ. J Biol Chem 272:20070–20076.

Millat G, Chikh K, Naureckiene S, Sleat DE, Fensom AH, Higaki K, Elleder M, Lobel P, Vanier MT (2001) Niemann-Pick disease type C: spectrum of HE1 mutations and genotype/phenotype correlations in the NPC2 group. Am J Hum Genet 69:1013–1021.

Naureckiene S, Sleat DE, Lackland H, Fensom A, Vanier MT, Wattiaux R, Jadot M, Lobel P (2000) Identification of HE1 as the second gene of Niemann-Pick C disease. Science 290:2298–2301.

Olsson S, Sundler R (2006) The role of lipid rafts in LPS-induced signaling in a macrophage cell line. Mol Immunol 43:607–612.

Patel SC, Suresh S, Kumar U, Hu CY, Cooney A, Blanchette-Mackie EJ, Neufeld EB, Patel RC, Brady RO, Patel YC, Pentchev PG, Ong WY (1999) Localization of Niemann-Pick C1 protein in astrocytes: implications for neuronal degeneration in Niemann-Pick type C disease. Proc Natl Acad Sci USA 96:1657–1662.

Patterson MC, Vanier MT, Suzuki K, Morris JA, Carstea ED, Neufeld EB, Blanchette-Mackie EJ, Pentchev PG (2001) Niemann-Pick disease type C: a lipid trafficking disorder. In: The metabolic and molecular bases of inherited disease (Scriver CR, Beaudet AL, Sly WS, Valle D, eds), pp 3611–3633. New York: McGraw-Hill.

Penkowa M, Molinero A, Carrasco J, Hidalgo J (2001) Interleukin-6 deficiency reduces the brain inflammatory response and increases oxidative

stress and neurodegeneration after kainic acid-induced seizures. Neuroscience 102:805–818.

Saito Y, Suzuki K, Nanba E, Yamamoto T, Ohno K, Murayama S (2002) Niemann-Pick type C disease: accelerated neurofibrillary tangle formation and amyloid β deposition associated with apolipoprotein E ε4 homozygosity. Ann Neurol 52:351–355.

Schindler C (1999) Cytokines and JAK/STAT signaling. Exp Cell Res 253:7–14.

Sugimoto Y, Ninomiya H, Ohsaki Y, Higaki K, Davies JP, Ioannou YA, Ohno K (2001) Accumulation of cholera toxin and GM1 ganglioside in the early endosome of Niemann-Pick C1-deficient cells. Proc Natl Acad Sci USA 98:12391–12396.

Suzuki K, Parker CC, Pentchev PG, Katz D, Ghetti B, D'Agostino AN, Carstea ED (1995) Neurofibrillary tangles in Niemann-Pick disease type C. Acta Neuropathol (Berl) 89:227–238.

Triantafilou M, Miyake K, Golenbock DT, Triantafilou K (2002) Mediators of innate immune recognition of bacteria concentrate in lipid rafts and facilitate lipopolysaccharide-induced cell activation. J Cell Sci 115:2603–2611.

Visintin A, Latz E, Monks BG, Espevik T, Golenbock DT (2003) Lysines 128 and 132 enable lipopolysaccharide binding to MD-2, leading to Toll-like receptor-4 aggregation and signal transduction. J Biol Chem 278:48313–48320.

Walker JG, Ahern MJ, Coleman M, Weedon H, Papangelis V, Beroukas D, Roberts-Thomson PJ, Smith MD (2006) Expression of Jak3, STAT1, STAT4 and STAT6 in inflammatory arthritis: unique Jak3 and STAT4 expression in dendritic cells in seropositive rheumatoid arthritis. Ann Rheum Dis 65:149–156.

Walkley SU, Suzuki K (2004) Consequences of NPC1 and NPC2 loss of function in mammalian neurons. Biochim Biophys Acta 1685:48–62.

Wu YP, Mizukami H, Matsuda J, Saito Y, Proia RL, Suzuki K (2005) Apoptosis accompanied by up-regulation of TNF-α death pathway genes in the brain of Niemann-Pick type C disease. Mol Genet Metab 84:9–17.

Yamamoto T, Ninomiya H, Matusmoto M, Ohta Y, Nanba E, Tsutsumi Y, Yamakawa K, Millat G, Vanier MT, Pentchev PG, Ohno K (2000) Genotype-phenotype relationship of Niemann-Pick disease type C: a possible correlation between clinical onset and levels of NPC1 protein in isolated skin fibroblasts. J Med Genet 37:707–712.

Zanjani TM, Sabetkasaei M, Mosaffa N, Manaheji H, Labibi F, Farokhi B (2006) Suppression of interleukin-6 by minocycline in a rat model of neuropathic pain. Eur J Pharmacol 538:66–72.

Cholesterol depletion facilitates ubiquitylation of NPC1 and its association with SKD1/Vps4

Yuki Ohsaki[1], Yuko Sugimoto[1], Michitaka Suzuki[1], Hiroshi Hosokawa[2], Tamotsu Yoshimori[3], Joanna P. Davies[4], Yiannis A. Ioannou[4], Marie T. Vanier[5], Kousaku Ohno[6] and Haruaki Ninomiya[1,*]

[1]Department of Neurobiology, Tottori University Faculty of Medicine, Yonago 683-8503, Japan
[2]Department of Intelligence Science and Technology, Graduate School of Informatics, Kyoto University, Kyoto 606-8501, Japan
[3]Department of Cell Genetics, National Institute of Genetics, Mishima 411-8540, Japan
[4]Department of Human Genetics, Mount Sinai School of Medicine, New York, NY 10029, USA
[5]INSERM Unit 189, Lyon-Sud Medical School and Fondation Gillet-Merieux, Lyon-Sud Hospital, 69921 Oullins, France
[6]Department of Child Neurology, Tottori University Faculty of Medicine, Yonago 683-8503, Japan
*Author for correspondence (e-mail: ninomiya@grape.med.tottori-u.ac.jp)

Accepted 23 March 2006
Journal of Cell Science 119, 2643-2653 Published by The Company of Biologists 2006
doi:10.1242/jcs.02993

Summary

Niemann-Pick disease type C (NPC) is an inherited lipid storage disorder caused by mutations in *NPC1* or *NPC2*. NPC1 is a polytopic glycoprotein that contains a sterol-sensing domain, whereas NPC2 is a soluble protein that contains an MD-2-like lipid-recognition domain. In the current study, we addressed the hypothesis that ubiquitylation of NPC1 might be regulated by cholesterol. We found that depletion of cellular cholesterol facilitated ubiquitylation of NPC1 expressed in COS cells. A loss-of-function mutant, NPC1(P691S), which contains an amino acid substitution in the sterol-sensing domain, failed to respond to cholesterol depletion. Another mutant, NPC1(δLLNF), which lacks the endosomal-targeting motif, also failed to respond. SKD1(E235Q), a dominant-negative mutant of SKD1/Vps4 that inhibits disassembly of the endosomal sorting complex required for transport (ESCRT), caused an accumulation of ubiquitylated NPC1. SKD1(E235Q) associated with NPC1 on the endosomal membrane, whereas wild-type SKD1 associated with NPC1 only when cells were depleted of cholesterol. Similarly, in control human skin fibroblasts, cholesterol depletion facilitated ubiquitylation of endogenous NPC1. In patient cells that lack NPC2 function, NPC1 was ubiquitylated regardless of cellular cholesterol levels, suggesting that NPC2 is required to prevent NPC1 ubiquitylation under cholesterol-rich conditions. These results suggest that ubiquitylation of NPC1 and its association with the ESCRT complex are controlled by endosomal cholesterol levels utilizing a mechanism that involves NPC2.

Key words: NPC1, NPC2, SKD1, Vps4, Ubiquitin, Cholesterol

Introduction

Niemann-Pick disease type C (NPC) is an autosomal recessive lipid storage disorder that is characterized by endosomal accumulation of low-density lipoprotein (LDL)-derived cholesterol (Patterson et al., 2001) and is caused by mutations in *NPC1* or *NPC2* (Carstea et al., 1997; Naureckiene et al., 2000). NPC1 is a membrane protein that resides primarily in the late endosome (Higgins et al., 1999), whereas NPC2 is a soluble protein that resides primarily in the lysosome (Vanier and Millat, 2004). These two proteins have been shown to function in the same endosomal cholesterol efflux pathway (Sleat et al., 2004). However, it is not clear how they interact with each other.

Solution of the human NPC1 membrane topology revealed a 1278 amino acid protein with 13 transmembrane domains and a sterol-sensing domain (SSD) located from transmembrane domains III to VII (Davies and Ioannou, 2000). Although this protein has been shown to possess a lipid permease activity (Davies et al., 2000) and the functional significance of its SSD has been well documented (Watari et al., 1999a; Millard et al., 2005), it is not known whether NPC1 function is regulated by cellular cholesterol. In addition to NPC1, SSDs are found in other proteins involved in the control of cellular cholesterol homeostasis: sterol regulatory element binding protein (SREBP) cleavage-activating protein (SCAP) and 3-hydroxy-3-methylglutaryl CoA reductase (HMG-CoAR), both of which reside primarily in the endoplasmic reticulum (ER). SCAP associates with the ER-retention proteins, Insig-1 and Insig-2, in a sterol-dependent manner: when cells are depleted of cholesterol, SCAP, together with SREBP, is released from the Insig proteins and transported to the Golgi apparatus, where a mature, active form of SREBP is generated by proteolysis and stimulates transcription of a diverse set of genes involved in cholesterol uptake and synthesis (Yang et al., 2002; Yabe et al., 2002). Similarly, HMG-CoAR associates with the Insig proteins in a sterol-dependent manner, but in this case, the association facilitates its ubiquitylation and subsequent degradation by the proteasome, thus shutting off endogenous cholesterol biosynthesis (Ravid et al., 2000; Sever et al., 2003a; Sever et al., 2003b). By analogy, one might hypothesize a cholesterol-dependent regulation of NPC1 function, either by its association with other proteins or by post-translational modifications.

Yeast genetic analysis has identified a number of proteins required for trafficking of endosomal proteins to the vacuole,

collectively termed the vacuolar protein sorting (Vps) proteins. These proteins assemble on the endosomal membrane to form the protein complexes ESCRT (endosomal sorting complex required for transport) -I, -II and -III, which operate sequentially (Katzmann et al., 2001; Babst et al., 2002a; Babst et al., 2002b). In this sorting process, ubiquitylation of an endosomal membrane protein serves as a signal for its sorting into the internal membranes of multivesicular bodies (Hicke, 2001). Vps4 is an ATPase that exists primarily in an inactive, ADP-bound cytosolic form and its active, ATP-bound form can transiently associate with the endosomal membrane. This protein is required for disassembly of the ESCRT-III. Expression of an ATPase-deficient, dominant-negative mutant of Vps4, the E233Q mutant, results in entrapment of ubiquitylated proteins on the endosomal membrane (Babst et al., 1997; Babst et al., 1998). Ncr1 is the yeast homolog of NPC1 and recent studies provided two lines of evidence that indicated a functional interaction between Ncr1 and Vps4. First, the targeting of Ncr1 to the vacuolar limiting membrane depends on Vps proteins, including Vps4 (Zhang et al., 2004). Second, Ncr1-null and Vps4-null cells share the same phenotype – resistance to the ether lipid drug edelfosine (Berger et al., 2005).

Mammalian counterparts to Vps proteins are presumed to function in a similar manner, and have been shown to be required for the ubiquitin-dependent, lysosomal transport of various membrane proteins, such as epidermal growth factor receptor (EGFR) (Bishop and Woodman, 2000; Bishop et al., 2002), G-protein-coupled receptors (Shenoy et al., 2001) and the cystic fibrosis transmembrane conductance regulator (Sharma et al., 2004). The suppressor of potassium transport growth defect protein 1, SKD1, is a mammalian ortholog of Vps4 and is a member of the *N*-ethylmaleimide-sensitive factor and AAA-type ATPase family (Scheuring et al., 2001). Like Vps4 in yeasts, SKD1 shuttles between an ADP-bound cytosolic form and an ATP-bound membrane-associated form. Also, similar to Vps(E233Q), SKD1(E235Q) lacks the ATPase activity and has a dominant-negative effect when expressed in mammalian cells. Expressed SKD1(E235Q) protein disrupts endosomal trafficking and localizes to aberrant endosomes (Yoshimori et al., 2000; Fujita et al., 2003).

Given the presence of an SSD, we hypothesized that NPC1 might be ubiquitylated by a cholesterol-dependent mechanism. Following confirmation that cellular cholesterol depletion facilitated NPC1 ubiquitylation, we pursued the hypothesis further that NPC1 interacts with the ESCRT complex.

Results

Cholesterol depletion facilitated ubiquitylation of NPC1 expressed in COS cells

NPC1 ubiquitylation was examined in COS cells transfected with Flag-NPC1 and myc/His_6-ubiquitin. 48 hours after transfection, cells were incubated either in cholesterol-rich medium [DMEM + 10% bovine calf serum (BCS)] or cholesterol-depleted medium [DMEM + 10% lipoprotein-deficient serum (LPDS)] supplemented with compactin and mevalonate. When cells were incubated in the cholesterol-depleted medium, the total cellular cholesterol level decreased in a time-dependent manner to reach ~60% of the control level at 12 hours. The cholesterol level was restored by supplementation with 20 μg/ml LDL (Fig. 1A). Expressed Flag-NPC1 was recovered by immunoprecipitation with anti-Flag M2 agarose and the products were analyzed by immunoblotting. As expected, Flag-NPC1 was detected in the immunoprecipitation products as a broad band between 150 and 250 kDa, as a result of its extensive glycosylation (Watari et al., 1999a). In addition, a band just below the top of the gel was often observed (for example, see Fig. 1E), which might represent an oligomerized form of the protein. Cholesterol depletion had little, if any, effect on the steady-state levels of the expressed proteins. However, probing with anti-myc revealed that cholesterol depletion caused conjugation of myc/His_6-ubiquitin to Flag-NPC1 (Fig. 1B). The positive signals were constantly detected at 6 hours and were sustained up to 24 hours. The conjugation was also demonstrated by metal affinity purification of myc/His_6-ubiquitin. Flag-NPC1 was detectable in the affinity purification products from cholesterol-depleted cells (Fig. 1C, left panel). Probing the affinity purification products with anti-myc showed no overall increase of ubiquitylated proteins in cholesterol-depleted cells (Fig. 1C, right panel). To see whether the ubiquitylation was caused by overexpression of ubiquitin molecules, cells were transfected only with Flag-NPC1 construct. Probing the anti-Flag immunoprecipitation products with anti-ubiquitin P4D1 revealed conjugation of endogenous ubiquitin to Flag-NPC1 in cells depleted of cholesterol (Fig. 1D).

Next, by using myc/His_6-ubiquitin co-expression, we examined whether cholesterol, instead of LDL, could suppress Flag-NPC1 ubiquitylation. Supplementation of the cholesterol-depleted medium with free cholesterol caused dose-dependent suppression of Flag-NPC1 ubiquitylation (Fig. 1E), suggesting that the ubiquitylation was a result primarily to cholesterol depletion.

To characterize Flag-NPC1 ubiquitylation further, we conducted two lines of experiments, first to examine effects of U18666A and second to examine detergent solubility of ubiquitylated Flag-NPC1. U18666A is a sterol derivative that has been shown to induce an NPC-like phenotype (Ko et al., 2001). To see whether this compound affected Flag-NPC1 ubiquitylation, transfected cells were incubated with 2 μg/ml U18666A for 12 hours. U18666A treatment at this concentration and duration caused endosomal cholesterol accumulation as revealed by filipin staining (data not shown) and, as reported previously (Sugimoto et al., 2001), an increase in the steady-state levels of expressed Flag-NPC1. Despite its effects on the steady-state levels, U18666A did not affect Flag-NPC1 ubiquitylation in cholesterol-rich medium nor did it suppress Flag-NPC1 ubiquitylation in cholesterol-depleted medium (Fig. 1F).

Cholesterol is the major constituent of raft microdomains and a part of NPC1 has been shown to associate with these domains (Garver et al., 2000). Therefore, it was possible that cholesterol depletion changed distribution of Flag-NPC1, which might lead to its ubiquitylation. To test this possibility, we examined the levels of Flag-NPC1 and its ubiquitylated form in 1% Triton X-100-soluble and Triton X-100-insoluble fractions, since raft microdomains are preferentially recovered in the insoluble fractions (Simons and Ikonen, 1997). Incubation for 6 hours in the cholesterol-depleted medium

reduced the level of Flag-NPC1 recovered from insoluble fractions. However, ubiquitylated Flag-NPC1 was recovered both from soluble and insoluble fractions (Fig. 1G). These data did not support the notion that Flag-NPC1 ubiquitylation was secondary to re-distribution of the protein between raft and non-raft membrane domains.

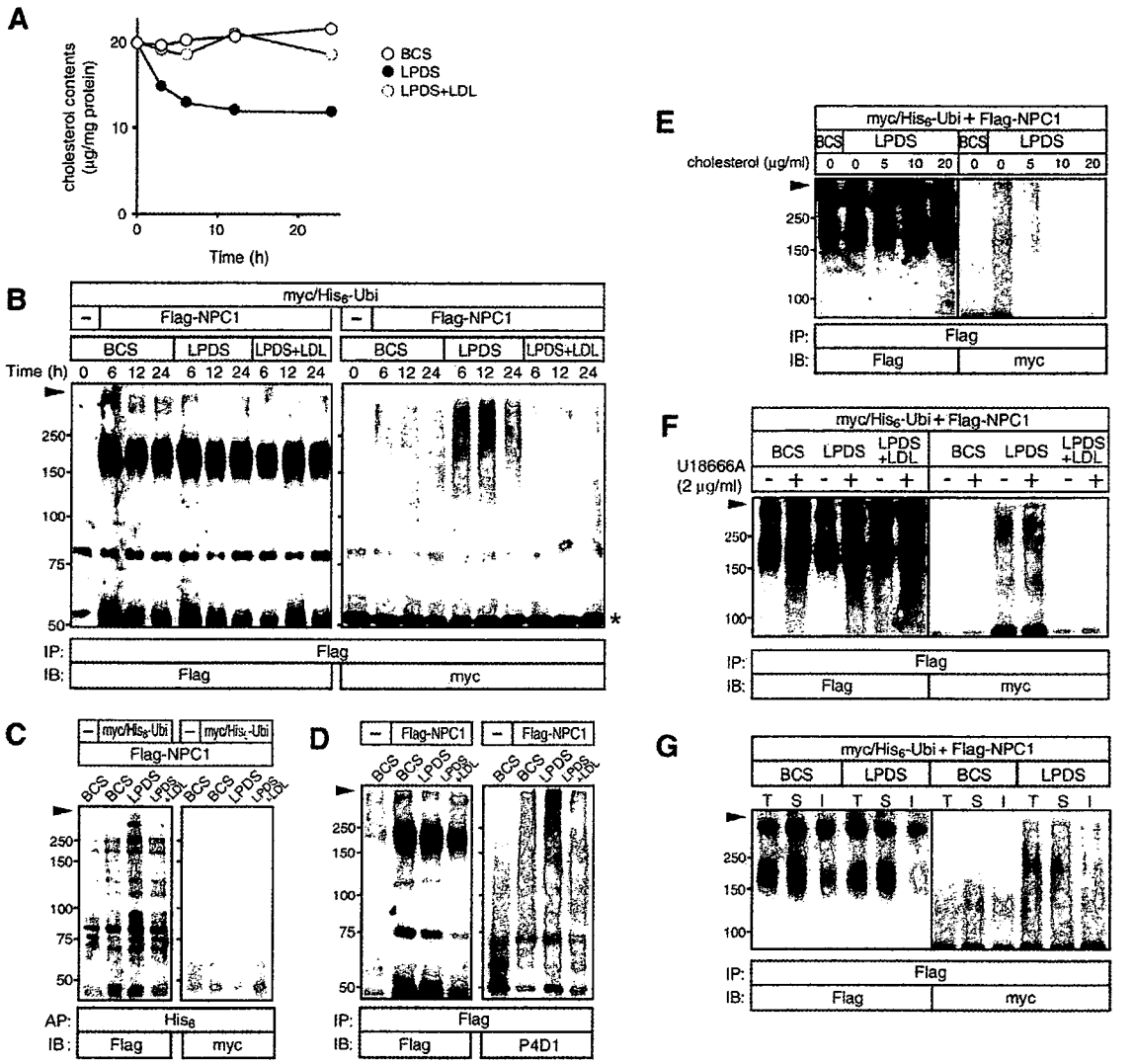

Fig. 1. Effects of cholesterol depletion on ubiquitylation of Flag-NPC1 expressed in COS cells. (A) Cellular cholesterol levels. Cells were cultured in cholesterol-rich medium (DMEM + 10% BCS) or cholesterol-depleted medium (DMEM + 10% LPDS supplemented with compactin and mevalonate) with or without LDL (20 μg/ml) up to 24 hours. Concentrations of total cholesterol in cell lysates were determined as described in the Materials and Methods. Each point represents the mean of duplicated determinations obtained in a single experiment. (B) Conjugation of myc/His_6-ubiquitin (myc/His_6-Ubi) to Flag-NPC1. Cells were transfected with expression constructs for myc/His_6-ubiquitin together with Flag-NPC1 or an empty vector. 48 hours after transfection, they were further cultured in the indicated medium. 0.5% CHAPS extracts were subjected to anti-Flag immunoprecipitation (IP) followed by immunoblotting (IB) with indicated antibodies. Molecular weights are given on the left (kDa). The arrowhead indicates the top of the separating gel and the asterisk indicates the heavy chain. (C) Co-purification of Flag-NPC1 with myc/His_6-ubiquitin. After incubation in the indicated medium for 6 hours, cell extracts were subjected to affinity purification with metal resin followed by immunoblotting with indicated antibodies. (D) Conjugation of endogenous ubiquitin to Flag-NPC1. Cells were transfected with Flag-NPC1 or an empty vector, cultured in the indicated medium for 6 hours and anti-Flag IP products were analyzed by indicated antibodies. (E) Effects of exogenous cholesterol on ubiquitylation of Flag-NPC1. Cells were transfected with myc/His_6-ubiquitin and Flag-NPC1, and cultured for 6 hours in cholesterol-rich or cholesterol-depleted medium supplemented with increasing concentrations of cholesterol. (F) Effects of U18666A. The transfected cells were cultured in the indicated medium for 12 hours in the presence or absence of U18666A. (G) Solubility of Flag-NPC1 to 1% Triton X-100. The transfected cells were cultured in the indicated medium for 6 hours. Total cell extracts (T), 1% Triton X-100-soluble (S) and Triton X-100-insoluble (I) fractions were prepared as described in the Materials and Methods. In E-G, anti-Flag immunoprecipitation products were subjected to immunoblotting with anti-Flag or anti-myc. All results shown are representative and were reproduced at least twice.

Mutant proteins Flag-NPC1(P691S) and Flag-NPC1(δLLNF) failed to respond to cholesterol depletion

To examine the role of the SSD in the cholesterol-level-dependent ubiquitylation, myc/His_6-ubiquitin co-expression experiments were repeated using Flag-NPC1(P691S), a loss-of-function mutant that contains an amino acid substitution in its SSD (Watari et al., 1999a; Millard et al., 2005). Anti-Flag immunoprecipitation products contained similar levels of Flag-NPC1 wild-type (wt) and P691S mutant proteins. Probing with anti-myc demonstrated that, in contrast to the wt protein, ubiquitylation of this mutant protein was barely facilitated following cholesterol depletion for 6 hours (Fig. 2A). To examine whether endosomal localization was required for NPC1 to undergo this modification, we examined effects of cholesterol depletion on the δLLNF mutant protein that lacks the C-terminal di-leucine motif and is retained in the ER (Watari et al., 1999b; Scott et al., 2004). As in the case of the P691S mutant, ubiquitylation of this mutant protein was barely affected by cholesterol depletion (Fig. 2B).

As a control experiment, we examined the effects of MG132, a proteasome inhibitor, on ubiquitylation of expressed proteins and found similar responses of the wt and mutant proteins. Similar to the wt protein, both P691S and δLLNF mutant proteins were extensively ubiquitylated in cells treated with 5 μM MG132 for 6 hours (Fig. 2).

Effects of MG132 and leupeptin on ubiquitylation of NPC1

Ubiquitylation can serve as a signal for protein degradation, which is executed by the cytosolic proteasome or by the lysosome. In an attempt to see whether ubiquitylated NPC1 underwent proteasomal and/or lysosomal degradation, we compared effects of MG132 and the lysosomal inhibitor leupeptin on Flag-NPC1 ubiquitylation. Treatment with 5 μM MG132 for 6 hours caused accumulation of ubiquitylated Flag-NPC1 and its effects were not influenced by cellular cholesterol levels. This increase in ubiquitylated Flag-NPC1 was accompanied by increased steady-state levels of Flag-NPC1, again regardless of the cholesterol levels (Fig. 3, upper panel). Similar results were reproduced with the proteasome inhibitor lactocystin (10 μM) (data not shown). By contrast, treatment with 100 μM leupeptin for 6 hours did not affect ubiquitylation of Flag-NPC1 either in cholesterol-rich or cholesterol-depleted conditions, nor caused appreciable changes in the steady-state levels of the protein (Fig. 3, lower panel). Incubation of the cells with NH_4Cl (10 mM for 6 hours) also failed to affect ubiquitylation of Flag-NPC1 and its steady-state levels (data not shown).

Interaction between SKD1(E235Q) and NPC1

Ubiquitylation can serve as a signal for the intracellular sorting of a protein. Since NPC1 resides primarily in the late endosome, we hypothesized that NPC1 was recognized by the ESCRT complex, which plays an essential role in the lysosomal sorting of ubiquitylated endosomal proteins. To address this hypothesis, NPC1 ubiquitylation was examined in the presence of SKD1(E235Q) (Fig. 4A), which inhibits disassembly of the ESCRT complex. When transfected cells were cultured in cholesterol-rich medium, expression of His_6-SKD1wt did not affect ubiquitylation of Flag-NPC1, whereas expression of His_6-SKD1(E235Q) caused a clear increase in the level of ubiquitylated Flag-NPC1 (Fig. 4B). Given its

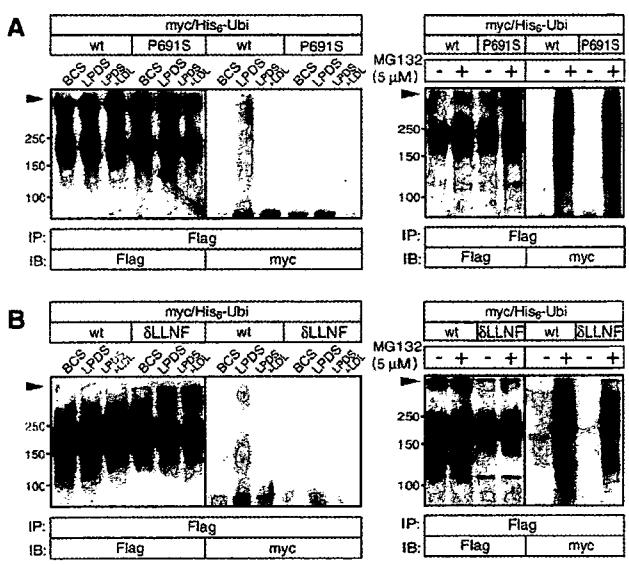

Fig. 2. Ubiquitylation of mutant NPC proteins. COS cells were transfected with myc/His_6-ubiquitin (myc/His_6-Ubi) together with Flag-NPC1 constructs that encoded the wild-type (wt) or mutant proteins P691S (A) or δLLNF (B); the arrowhead indicates the top of the separating gel. Cells were cultured in the indicated medium for 6 hours (left panels) or treated with or without MG132 for 6 hours (right panels). In both A and B, anti-Flag immunoprecipitation (IP) products were subjected to immunoblotting (IB) with anti-Flag or anti-myc. All results shown are representative and were reproduced at least twice.

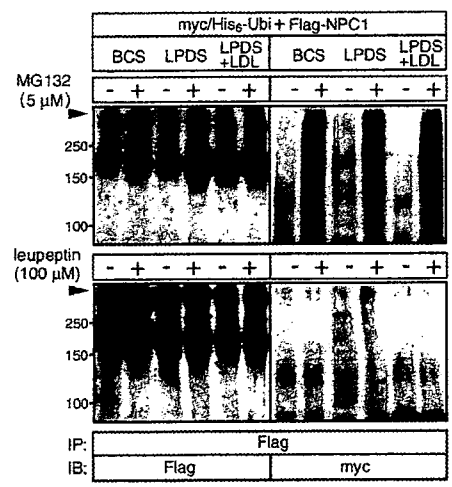

Fig. 3. Effects of MG132 and leupeptin on ubiquitylation of Flag-NPC1. COS cells were transfected with myc/His_6-ubiquitin (myc/His_6-Ubi) and Flag-NPC1 constructs, and were cultured in the indicated medium for 6 hours in the absence or presence of MG132 (upper panel) or leupeptin (lower panel); the arrowhead indicates the top of the separating gel. Anti-Flag immunoprecipitation (IP) products were subjected to immunoblotting (IB) with anti-Flag or anti-myc. All results shown are representative and were reproduced at least twice.

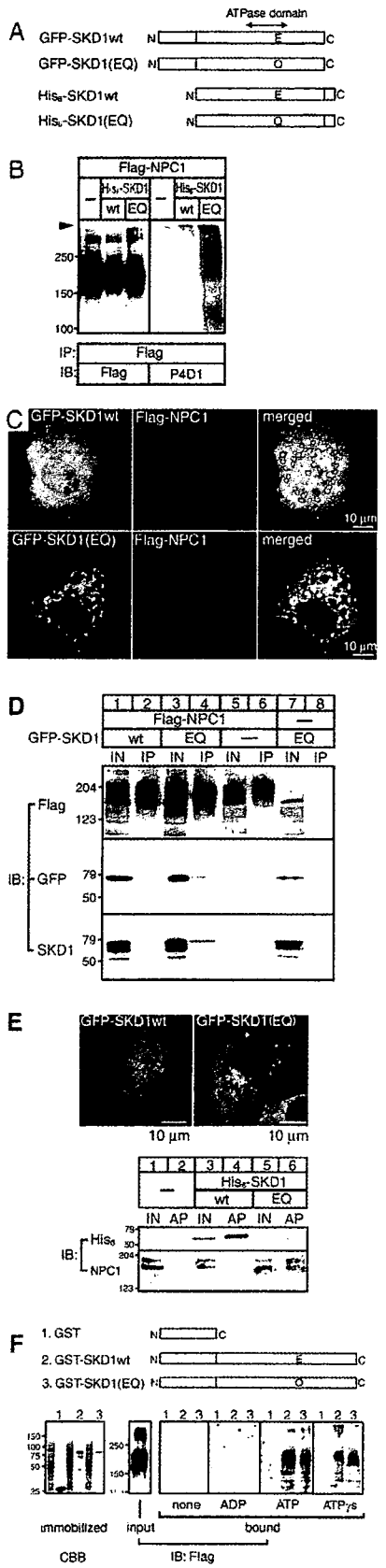

effects on NPC1 ubiquitylation, we examined whether SKD1(E235Q) co-localized and could interact with NPC1. Expression of a GFP-SKD1wt construct yielded a diffuse distribution in the cytoplasm and the nucleus, and did not induce any obvious changes of intracellular structures. Anti-Flag immunofluorescence revealed that Flag-NPC1 was retained in endosomes and did not co-localize with GFP-SKD1wt. As reported previously (Yoshimori et al., 2000; Fujita et al., 2003), expression of GFP-SKD1(E235Q) results in the formation of multiple aberrant vesicles that associated with the E235Q protein. Flag-NPC1 also localized to these aberrant endosomes and partially co-localized with GFP-SKD1(E235Q) (Fig. 4C). Detection of His_6-tagged SKD1 and Flag-NPC1 proteins yielded similar results (data not shown).

We next examined whether there was any interaction between Flag-NPC1 and SKD1 by immunoprecipitation and immunoblotting experiments. Similar levels of Flag-NPC1 were recovered by anti-Flag immunoprecipitation from cells expressing wt or E235Q mutant GFP-SKD1 protein (Fig. 4D, lanes 2 and 4). Probing the same immunoprecipitation products with anti-GFP showed that a portion of the GFP-SKD1(E235Q) protein was co-precipitated with Flag-NPC1

Fig. 4. Interaction between SKD1(E235Q) and NPC1. (A) Schematic representation of expressed SKD1 proteins. Each tag is shown in gray. (B) Flag-NPC1 ubiquitylation. COS cells were transfected with the Flag-NPC1 construct together with an empty vector or His_6-SKD1 constructs. 48 hours after transfection, anti-Flag immunoprecipitation (IP) products were subjected to immunoblotting (IB) with anti-Flag or anti-ubiquitin (P4D1). Molecular weights are given on the left (kDa); the arrowhead indicates the top of the separating gel. (C) Intracellular localization of GFP-SKD1 and Flag-NPC1. COS cells expressing Flag-NPC1 and GFP-SKD1 wild-type (wt; upper) or the E235Q mutant (EQ; lower) were fixed and stained with anti-Flag antibody. Bound antibody was visualized with Alexa Fluor 546-conjugated secondary antibody. Results shown are the representative images obtained with a confocal microscope. (D) Co-precipitation of Flag-NPC1 and GFP-SKD1 proteins. 0.5% CHAPS extracts were prepared from COS cells transfected with Flag-NPC1 together with GFP-SKD1wt or E235Q constructs. Anti-Flag immunoprecipitation products were analyzed by immunoblotting with the indicated antibodies. Cell extracts (IN: input) were loaded on lanes 1, 3, 5 and 7, and corresponding immunoprecipitation products were loaded on lanes 2, 4, 6 and 8. (E) Co-purification of endogenous NPC1 in CHO cells with His_6-SKD1 proteins. Upper; intracellular localization of GFP-SKD1. Results shown are the representative images obtained with a confocal microscope. Lower; affinity purification. 0.5% CHAPS extracts were prepared from cells transfected with an empty vector, His_6-SKD1wt or E235Q constructs. His_6-tagged proteins were affinity purified with metal affinity resin and were analyzed by immunoblotting with the indicated antibodies. Cell extracts (IN; input) were loaded on lanes 1, 3 and 5, and corresponding affinity-purification products (AP) were loaded on lanes 2, 4 and 6. (F) In vitro interaction between GST-SKD1 and Flag-NPC1. GST-fused proteins, as shown in the schematic representations, were expressed in *E. coli* and immobilized on glutathione sepharose (left, CBB: Coomassie Blue staining). 0.5% CHAPS extracts (input) were prepared from COS cells expressing Flag-NPC1. Cell extracts were incubated with immobilized GST-fused proteins in the absence or presence of 0.5 mM ADP, ATP or ATPγs. Bound proteins were eluted with glutathione and analyzed by anti-Flag immunoblotting (right). Molecular weights are given on the left (kDa). All results shown are representative and were reproduced at least twice.

(lane 4), whereas no GFP-SKD1wt could be co-precipitated (lane 2). These results were confirmed by probing with anti-SKD1 (lanes 2 and 4). Of note, in addition to GFP-SKD1 at 78 kDa, the anti-SKD1 antibody detected the endogenous SKD1 at 52 kDa (lanes 1, 3, 5 and 7), which, as expected, was not co-precipitated with Flag-NPC1 (lanes 2, 4 and 6). Further confirmation of the results was provided by repeating the above experiments using extracts from cells expressing His_6-tagged SKD1 proteins (data not shown).

Because CHO cells express a readily detectable level of NPC1 (Higaki et al., 2001), we used this cell line to test whether SKD1(E235Q) could interact with endogenous NPC1 (Fig. 4E). Unlike Flag-NPC1 expressed in COS cells, endogenous NPC1 in CHO cells exhibited relatively sharp bands with molecular weights of 170 and 200 kDa. Expression of GFP-SKD1(E235Q), but not GFP-SKD1, again caused the formation of aberrant endosomes containing the mutant protein. These results could be reproduced using His_6-tagged SKD1 proteins (data not shown). When the His_6-tagged SKD1 protein was affinity purified from cell extracts using metal affinity chromatography, a portion of endogenous NPC1 was co-purified with His_6-SKD1(E235Q) (Fig. 4E, lane 6), but not with His_6-SKD1wt (lane 4).

Although the above findings suggested an interaction between NPC1 and the ATP-bound, membrane-associated form of SKD1, it was possible that this interaction was secondary to the formation of the aberrant vesicles that are known to accumulate various endosomal proteins (Yoshimori et al., 2000; Fujita et al., 2003). To address this question, we examined whether NPC1 could bind to SKD1 in vitro (Fig. 4F). Human wt and E235Q mutant SKD1 proteins were expressed as GST-fusion proteins in *Escherichia coli*, whereas Flag-NPC1 was expressed and detergent solubilized from COS cells. GST-SKD1 proteins were immobilized on glutathione sepharose and incubated with 0.5% CHAPS-solubilized cell extracts. Flag-NPC1 bound to the sepharose with binding to both GST-SKD1wt and the E235Q mutant dependent on the presence of ATP or ATPγs. No binding could be detected in the presence of ADP.

Cholesterol depletion facilitated the interaction between NPC1 and wt SKD1

The above findings indicated that NPC1 could interact with the ATP-bound, membrane-associated form of SKD1. To address whether this interaction occurred in cholesterol-depleted cells, cells expressing Flag-NPC1 and His_6-SKD1wt were cultured in cholesterol-depleted medium. In these cells, there was an increase in the amount of His_6-SKD1wt that co-precipitated with Flag-NPC1, as compared with the level in cells cultured in cholesterol-rich medium (Fig. 5A). This co-precipitation was largely suppressed by LDL supplementation of cholesterol-depleted medium.

These findings suggested that at least a part of His_6-SKD1wt was recruited to the endosomes of cholesterol-depleted cells. To confirm this, Opti-prep fractionation of cell homogenates was carried out to detect the membrane-associated form of SKD1 (Fig. 5B). Following fractionation, the endosomal marker protein lamp2 was mainly distributed in fractions 4-7 and cholesterol depletion caused a leftward shift of this distribution to fractions 4-6. Similar to lamp2, Flag-NPC1 was distributed in fractions 3-8 and in 3-7 for the cholesterol-rich

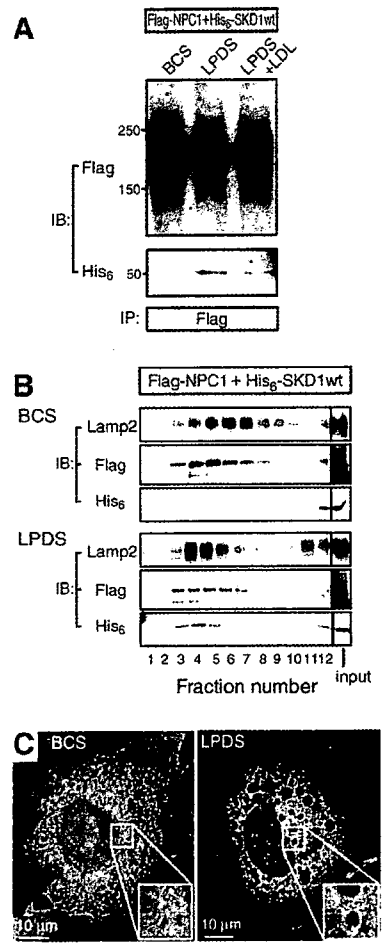

Fig. 5. Effects of cholesterol depletion on an interaction between Flag-NPC1 and wild-type SKD1. Transfected COS cells were cultured in cholesterol-rich or cholesterol-depleted medium with or without LDL for 16 hours. (A) Co-precipitation of His_6-SKD1wt with Flag-NPC1. Cells were transfected with His_6-SKD1wt together with Flag-NPC1 constructs. Anti-Flag immunoprecipitation (IP) products were analyzed by immunoblotting (IB) with the indicated antibodies. Molecular weights are given on the left (kDa). (B) Cell fractionation. Cells were transfected with Flag-NPC1 and His_6-SKD1wt constructs. Membrane fractions (100,000 *g* pellet) of cell homogenates were fractionated on an Opti-prep gradient. The fractions, together with the membrane fractions applied (input), were analyzed by immunoblotting with the indicated antibodies. Shown are representative results that were reproduced three times. (C) Intracellular localization of Flag-NPC1 and GFP-SKD1wt. Cells expressing Flag-NPC1 and GFP-SKD1wt were stained with anti-Flag antibody, and bound antibody was visualized with Alexa Fluor 546-conjugated secondary antibody. Results shown are the representative images obtained with a confocal microscope. Shown in the insets are the enlarged images of the indicated areas.

and cholesterol-depleted cell homogenates, respectively. Cholesterol depletion caused a more significant change in the distribution of His_6-SKD1wt. In cells cultured in cholesterol-rich medium, His_6-SKD1wt was exclusively recovered in the bottom fraction 12, whereas in cells cultured using cholesterol-depleted medium, this protein was also recovered in fractions

3-6. As a control experiment, we examined the distribution of His_6-SKD1(E235Q) and found that this protein was distributed in fractions 3-6 regardless of the cellular cholesterol levels (data not shown).

To confirm the endosomal recruitment of SKD1 in cholesterol-depleted cells further, we examined the intracellular localization of GFP-SKD1wt. As shown in Fig. 4C and Fig. 5C (left panel), when cells expressing Flag-NPC1 and GFP-SKD1wt were cultured in cholesterol-rich medium, GFP-SKD1wt was cytosolic and did not co-localize with endosomal Flag-NPC1. When these cells were cultured in cholesterol-depleted medium, GFP-SKD1wt was concentrated on the rim of enlarged endosomes where it co-localized with Flag-NPC1 (Fig. 5C, right panel).

Cholesterol depletion facilitated ubiquitylation of endogenous NPC1 and its association with SKD1 in controls but not in NPC human skin fibroblasts

The above findings indicated that cholesterol depletion induced ubiquitylation of NPC1 and its interaction with SKD1, when these proteins were expressed in COS cells. To examine whether cholesterol depletion had similar effects on endogenous NPC1 and SKD1, we used primary-cultured human skin fibroblasts from a control subject H34 and an NPC patient UCH (homozygous for the NPC1 H510P mutation). As reported previously (Yamamoto et al., 2000), UCH cells expressed undetectable levels of NPC1 (Fig. 6A), and were included as a negative control. Probing of H34 cell extracts with anti-NPC1 showed that, like CHO cells, these cells contained two species of NPC1 – a major band at 170 kDa and a minor band at 200 kDa – and that cholesterol depletion caused a marginal decrease in the steady-state levels of the NPC1 protein (Fig. 6A). Since immunoprecipitation of the endogenous NPC1 protein was unsuccessful, we employed anti-ubiquitin (P4D1) immunoprecipitation to evaluate the extent of NPC1 ubiquitylation (Fig. 6B). Probing with anti-NPC1 antibody showed that NPC1 was absent in the anti-ubiquitin immunoprecipitation products from cells cultured in cholesterol-rich medium, but was clearly detectable in the immunoprecipitation products from cells depleted of cholesterol. Probing of cell extracts with anti-ubiquitin antibody showed no overall increase of ubiquitylated proteins caused by cholesterol depletion (data not shown). The specificity of anti-NPC1 signals was confirmed by their absence in the immunoprecipitation products from UCH cells. Probing with anti-SKD1 antibody showed that cholesterol depletion increased the level of SKD1 contained in the anti-ubiquitin immunoprecipitation products from H34 cells. By contrast, cholesterol depletion did not alter the levels of SKD1 in the immunoprecipitation products from UCH cells.

Next, using Opti-prep fractionation, the recruitment of SKD1 to the endosomes of cholesterol-depleted cells was examined (Fig. 6C). Both lamp2 and NPC1 in membrane fractions of H34 cells were recovered in fractions 3-5 and, similar to the observations in COS cells (Fig. 5B), cholesterol depletion caused a leftward shift of this distribution to fractions 2 and 3. SKD1 was not recovered in these fractions when cells were cultured in cholesterol-rich medium, but was recovered in fractions 2 and 3 when cells were depleted of cholesterol.

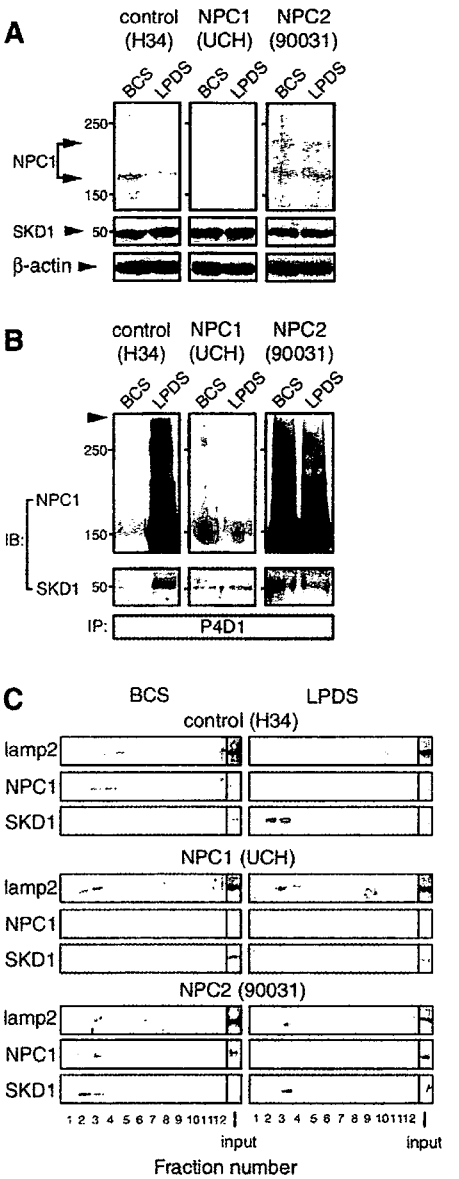

Fig. 6. Effects of cholesterol depletion on ubiquitylation of endogenous NPC1 and its interaction with SKD1 in human skin fibroblasts. Cells from a control subject or patients with NPC1 or NPC2 disease were cultured in cholesterol-rich or cholesterol-depleted medium for 16 hours. (A) Expression of NPC1 and SKD1. 0.5% CHAPS extracts were analyzed by immunoblotting (IB) with antibodies against the indicated proteins. (B) NPC1 ubiquitylation and its association with SKD1. 0.5% CHAPS extracts were subjected to anti-ubiquitin (P4D1) immunoprecipitation (IP) and the immunoprecipitated products were analyzed by immunoblotting with the indicated antibodies. Molecular weights are given on the left (kDa). (C) Cell fractionation. Membrane fractions (100,000 *g* pellet) of cell homogenates were fractionated on an Opti-prep gradient. All results shown are representative and were reproduced at least twice.

In membrane fractions of UCH cells, lamp2 was recovered in fractions 2 and 3 and, unlike in H34 cells, cholesterol depletion caused a rightward shift of this distribution to fractions 3-5. As

expected, NPC1 was absent in UCH cell fractions and, again unlike in H34 cells, SKD1 was not at all recovered in these fractions regardless of the cellular cholesterol levels.

It was possible that this lack of SKD1 recruitment in UCH cells was simply because the cells lacking NPC1 could not be effectively depleted of cholesterol. To address this issue, UCH cells were cultured in cholesterol-depleted medium for 3 days. This treatment abolished endosomal cholesterol accumulation as revealed by filipin staining but again failed to induce endosomal recruitment of SKD1 (data not shown). These findings suggested that the negative results in UCH cells were not a result of ineffective cholesterol depletion, but a result of the absence of NPC1.

Finally, to see if NPC2 is involved in the regulation of NPC1 ubiquitylation, we repeated the same experiments using cells from a patient with NPC2 disease (90031, homozygous for the NPC2 E20X mutation), which lack NPC2 function. Our previous analysis using 0.4% SDS extracts from 100,000 *g* membrane preparations revealed an increased amount of NPC1 in the NPC2 cells as compared with control cells (Millat et al., 2001a). However, anti-NPC1 blotting of 0.5% CHAPS extracts showed comparable levels of NPC1 between H34 and the NPC2 cells (Fig. 6A), suggesting reduced solubility of NPC1 in these cells to this detergent. Nonetheless, anti-ubiquitin immunoprecipitation experiments using the 0.5% CHAPS extracts revealed distinct patterns of NPC1 ubiquitylation. A part of NPC1 was ubiquitylated in these cells regardless of the cholesterol levels (Fig. 6B). This ubiquitylation of NPC1 was accompanied by the presence of SKD1 in the anti-ubiquitin immunoprecipitation products from cells cultured either in cholesterol-rich or cholesterol-depleted medium (Fig. 6B). Opti-prep fractionation of the NPC2 cells showed a distinct distribution pattern of SKD1. Both lamp2 and NPC1 were recovered in fractions 2 and 3 from cells cultured in cholesterol-rich medium and, unlike in H34 cells, cholesterol depletion caused a rightward shift of this distribution to fractions 3-5. In contrast to H34 cells, SKD1 co-localized with NPC1 regardless of the cellular cholesterol levels and it was present in fractions 2 and 3, and in 3-5, from cells cultured in cholesterol-rich and cholesterol-depleted medium, respectively (Fig. 6C). Similar results were obtained by using another NPC2 cell strain 88082 (data not shown), suggesting that they are a common feature of NPC2-deficient cells.

Discussion

The biochemical mechanism and physiological implication of the cholesterol-dependent control of protein ubiquitylation has so far been documented only for HMG-CoAR, a rate-limiting enzyme of cholesterol biosynthesis localized in the ER. Briefly, repletion of cellular cholesterol facilitates association of HMG-CoAR with the Insig proteins, which in turn accelerates its ubiquitylation and proteasomal degradation (Ravid et al., 2000; Sever et al., 2003a; Sever et al., 2003b). We have shown in the current study that ubiquitylation of NPC1 was induced by depletion of cellular cholesterol, but not by its repletion. It is currently unknown how cholesterol exerts opposite effects on NPC1 and HMG-CoAR, the two proteins that share SSDs. These opposite effects possibly result from differences in their subcellular locations and/or the nature of the interacting proteins involved in the regulatory processes. We have shown that two kinds of mutant NPC1 proteins – P691S and δLLNF – failed to respond to cholesterol depletion (Fig. 2). The negative response of the P691S mutant suggested that an intact SSD was required for NPC1 to undergo this modification, whereas the negative response of the δLLNF mutant suggested that the modification took place in the endosomes, where NPC1 normally resides.

Ubiquitylation of a protein can serve as a signal for its degradation or intracellular sorting. Unlike the case of HMG-CoAR, cholesterol-level-dependent NPC1 ubiquitylation does not appear to serve a major role in the control of protein degradation, since cholesterol depletion caused little effect on the steady-state levels of expressed Flag-NPC1 (Fig. 1). Its effect on the steady-state levels of endogenous NPC1 was also marginal (Fig. 6). This finding agrees with the observation by Zhang et al. (Zhang et al., 2001), who found negative effects of cholesterol depletion on the NPC1 protein levels in human skin fibroblasts. Ubiquitylated proteins can be degraded either by the lysosome or by the proteasome in the cytosol. The negative effects of the lysosomal inhibitor leupeptin on ubiquitylation of NPC1 and its steady-state levels (Fig. 3) argue against a role of the lysosome in NPC1 degradation. Our findings with the proteasomal inhibitor MG132 suggest that, like HMG-CoAR, NPC1 does undergo ubiquitylation and proteasomal degradation, but these events appear to be independent to cellular cholesterol levels. MG132 caused accumulation of ubiquitylated Flag-NPC1 and increased its steady-state levels regardless of cellular cholesterol levels (Fig. 3). MG132 induced ubiquitylation of the P691S and δLLNF mutant proteins that failed to respond to cholesterol depletion (Fig. 2). Therefore, as for the role of the proteasome in NPC1 degradation, we hypothesize that NPC1 undergoes ubiquitylation and proteasomal degradation because of protein misfolding, but not because of cholesterol depletion, and that the quality control takes place in the ER, but not in the endosome.

Our findings on the interaction between NPC1 and SKD1 suggest that ubiquitylation of NPC1 induced by cholesterol depletion serves as a sorting signal. The interaction between NPC1 and the ATP-bound, membrane-associated form of SKD1 was indicated by co-localization and co-precipitation of NPC1 and SKD1(E235Q) (Fig. 4C-E). This interaction only occurs with the ATP-bound form of SKD1, as shown by the in vitro binding of NPC1 to immobilized SKD1, which depended on the presence of ATP/ATPγs (Fig. 4F). Importantly, cholesterol depletion induced an interaction between NPC1 and wt SKD1, which presumably was in the ATP-bound, membrane-associated form (Fig. 5). The effect of cholesterol depletion on NPC1 ubiquitylation was also demonstrated for the endogenous protein in human skin fibroblasts (Fig. 6B) and, again, this ubiquitylation was accompanied by recruitment of SKD1 to the endosomal fractions (Fig. 6C). In yeast, Vps4 is required for disassembly of the ESCRT-III, which contains other Vps proteins Vps2, Vps20, Vps24 and Vps32/Snf7 (Babst et al., 2002a). Mammalian counterparts to these proteins have recently been identified (Fujita et al., 2004; Peck et al., 2004; Yan et al., 2005). Our findings suggest that NPC1 interacted with these proteins in the presence of SKD1(E235Q) or in cells depleted of cholesterol.

Two lines of questions can be addressed regarding the interaction between NPC1 and the ESCRT complex. First, how is ubiquitylated NPC1 recognized by the ESCRT complex?

Tsg101 is a mammalian ortholog of yeast Vps23 and has been shown to bind directly to ubiquitylated EGFR (Bishop and Woodman, 2001; Bishop et al., 2002). We tested whether Flag-NPC1 interacted with endogenous Tsg101 in COS cells, but could not detect any interaction between these two proteins. Therefore, it is likely that NPC1 is recognized by the ESCRT complex in a manner that is different to EGFR. Second, what is the role of the ESCRT complex in the intracellular sorting of NPC1? NPC1 is primarily localized on the late endosome and can transiently associate with cholesterol-enriched lysosomes (Higgins et al., 1999). The ESCRT complex plays a crucial role in the sorting of ubiquitylated proteins form the endosome to the lysosome through multivesicular bodies (Bishop and Woodman, 2000; Yoshimori et al., 2000; Bishop et al., 2002; Fujita et al., 2003) and, in Vps mutant yeast cells, Ncr1 is trapped in the pre-vacuolar compartments (Zhang et al., 2004), which correspond to mammalian endosomes. Therefore, it is likely that the ESCRT complex is required for the sorting of NPC1 from the late endosome to the lysosome. At least in yeast, it has been shown that the entry of the ubiquitylated protein to multivesicular bodies is preceded by de-ubiquitylation of the protein (Babst et al., 2002a). Given the effects of cholesterol depletion, we propose that the sorting of NPC1 is regulated by the local cholesterol content of the endosomal membrane. When it is low, NPC1 is ubiquitylated and is associated with the ESCRT complex. Its entry into multivesicular bodies and subsequent delivery to the lysosome might be triggered by cholesterol feeding, which presumably induces de-ubiquitylation of the protein. This sorting might be an obligatory step for the NPC1 function to relocate LDL-derived lysosomal cholesterol; further analysis is required to test our hypothesis.

Finally, our findings regarding the NPC2 cells provided an important insight into a functional relationship between NPC1 and NPC2. In cells that lack functional NPC2, ubiquitylation of NPC1 (Fig. 6B) and endosomal recruitment of SKD1 (Fig. 6C) occurred under cholesterol-rich conditions, similar to the results obtained in control cells depleted of cholesterol. Thus, under cholesterol-rich conditions, the presence of functional NPC2 was required to prevent NPC1 ubiquitylation and subsequent association with SKD1. NPC2 contains an MD-2-like lipid-recognition domain and binds cholesterol. By analogy to other proteins that contain this domain, it can be postulated that NPC2 extracts membrane-embedded cholesterol and makes it available to other proteins (Inohara and Nunez, 2002). Therefore, one possible explanation for NPC1 ubiquitylation in NPC2 cells is that cholesterol is unavailable to the membrane domains where NPC1 resides, inducing NPC1 modification that normally takes place under conditions of cholesterol deprivation. This explanation is consistent with the increased protein levels of NPC1 in NPC2 cells (Millat et al., 2001a), given that NPC1 ubiquitylation caused by cholesterol depletion does not lead to its degradation. Alternatively, it is also possible that NPC2 deficiency acts indirectly, by inducing aberrant compartmentalization of NPC1, and triggering its ubiquitylation. However, this alternative explanation does not agree with our observation that U18666A, which induces aberrant compartmentalization of NPC1, failed to affect its ubiquitylation (Fig. 1F). We suggest that cholesterol-level-dependent ubiquitylation of NPC1 is a crucial event not only to understand the intracellular sorting of NPC1 but also to unravel the functional relationship between NPC1 and NPC2 in future studies.

Materials and Methods

Materials

Dulbecco's modified Eagle's medium (DMEM), Ham's F12 medium and LipofectAMINE reagent were from Life Technologies. Bovine calf serum (BCS) was from Atlanta Biologicals. Bovine lipoprotein-deficient serum (LPDS), human LDL, anti-Flag M2 agarose and rabbit polyclonal anti-Flag antibody were from Sigma. Rabbit polyclonal anti-NPC1 antibody and mouse monoclonal antibodies against ubiquitin (P4D1), myc, His_6 and GFP were from Santa Cruz Biotech. Rabbit polyclonal anti-SKD1 has been described (Yoshimori et al., 2000).

Mammalian expression of recombinant proteins

pASC9/Flag-NPC1, an expression plasmid for human NPC1 with a Flag tag inserted in the *ClaI* site, has been described (Davies and Ioannou, 2000). pSV-SPORT/NPC1 wild-type (wt) and the P691S mutant were a gift from J. F. Strauss III (Department of Obstetrics and Gynecology, University of Pennsylvania School of Medicine, VA). The *PsyI* fragment of the Flag-NPC1 cDNA that flanks the Flag epitope was introduced to the corresponding site of pSV-SPORT/NPC1 wt and P691S to generate a Flag-tagged version of the cDNAs. The C-terminal 12 bp were deleted from pSV-SPORT/Flag-NPC1 by PCR-based mutagenesis to generate a cDNA that encoded Flag-NPC1(δLLNF). An expression plasmid for myc/His_6-tagged yeast ubiquitin was a gift from R. Kopito (Department of Biological sciences, Stanford University, CA). Expression plasmids for GFP-tagged mouse wt and E235Q mutant SKD1 have been described (Yoshimori et al., 2000). The entire coding sequence of human SKD1 cDNA (Vps4-B) (Scheuring et al., 2001) was obtained by RT-PCR with primers 5′-TCCGCCATGTCATCCACTTCG-3′ and 5′-GCTTTTGGCTTAG-CCTTCTTG-3′ from human skin fibroblasts cDNA. A His_6 epitope was introduced at the C-terminus by PCR and the cDNA was subcloned to the *EcoRI/XhoI* site of a mammalian expression vector pME18sf. An amino acid substitution E235Q was introduced to pME/His_6-SKD1 using a Quick Change Site-Directed mutagenesis kit (Stratagene) and was confirmed by direct sequencing. Cells were transfected using LipofectAMINE reagent according to the manufacturer's instructions.

Cell culture

COS cells and human skin fibroblasts were maintained in DMEM/10% BCS at 37°C in a humidified atmosphere containing 5% CO_2. Human skin fibroblasts were from a control human subject (H34), and from patients with NPC1 (UCH) (Yamamoto et al., 2000) and NPC2 (90031 and 88082) (Millat et al., 2001b) diseases. CHO cells were maintained in F12 medium as above. To deplete cellular cholesterol, cells were cultured for the time indicated in 10% LPDS supplemented with an HMG-CoAR inhibitor compactin (2 μM) and sodium mevalonate (0.1 mM), which assures cell viability (Ravid et al., 2000). Where indicated, this cholesterol-depleted medium was supplemented with 20 μg/ml LDL. For determination of cholesterol levels, cells in 6-well plates were scraped into PBS and lysed by sonication. Concentrations of protein and total cholesterol in the lysates were determined by using the microprotein assay kit (BioRad) and the Amplex red cholesterol assay kit (Molecular Probes), respectively, according to the manufacturer's instructions.

Immunoprecipitation and affinity purification

All procedures were carried out at 4°C. Cells were washed with PBS and lysed by sonication in buffer A [Tris-HCl 10 mM pH 7.4, NaCl 150 mM, 1 mM EDTA, 1 mM EGTA, 0.5% CHAPS and a protease inhibitor cocktail (Boehringer)]. After a brief centrifugation to remove insoluble material, the supernatant was precleared with an aliquot of agarose beads. For immunoprecipitation of Flag-NPC1, the extracts were incubated for 16 hours with anti-Flag M2 agarose beads, washed with buffer A, followed by elution of bound proteins by heating at 65°C for 10 minutes in SDS-PAGE sample buffer. SDS-PAGE, western transfer and immunoblotting were carried out as previously described (Sugimoto et al., 2001). The blot was developed using an ECL kit (Amersham Pharmacia). For immunoprecipitation of ubiquitylated proteins, cell extracts were incubated with anti-ubiquitin P4D1 antibodies for 16 hours and the immunoprecipitates were collected with protein A sepharose. For affinity purification of His_6-tagged proteins (myc/His_6-ubiquitin or His_6-SKD1), cell extracts were incubated for 16 hours with TALON metal affinity resin (Clontech). Bound proteins were analyzed as described above.

Cell fractionation

Cells were harvested in Tris-buffered saline (TBS; Tris-HCl 10 mM pH 7.4, NaCl 150 mM) supplemented with a protease inhibitor cocktail and lysed by sonication. The cell lysates were incubated on ice for 30 minutes in TBS supplemented with 1% Triton X-100 and 0.1% SDS to give total extracts. To prepare 1% Triton X-100-soluble and Triton X-100-insoluble fractions, the cell lysates were incubated in TBS + 1% Triton X-100 and, after centrifugation at 100,000 *g* for 30 minutes, the pellet was suspended in TBS + 1% Triton X-100 + 0.1% SDS. For subcellular fractionation, membranes were fractionated by using an Opti-prep gradient (Axis-